

Chapter 6

Zirconium Oxide (ZrO₂)

6.1 Introduction

Zirconium dioxide (ZrO₂), also known as Zirconia, is a white crystalline oxide of Zirconium. Its most naturally occurring form, with a monoclinic crystalline structure, is the rare mineral, baddeleyite. The high temperature cubic crystalline form, called 'cubic zirconia', is rarely found in nature as mineral tazheranite (Zr, Ti, Ca) O₂, but is synthesized in various colours for use as a gemstone. This cubic crystal structured variety cubic zirconia is the best-known diamond simulant.

As an important ceramic material, ZrO₂ has widespread potential applicability in the fields of structural materials, solid state electrolytes, thermal barrier coatings, electro-optical materials, gas sensing, corrosion resistance, and catalysis ^[1]. Zirconia coatings, due to their chemical stability, high coefficient of thermal expansion, low thermal conductivity and high thermo mechanical resistance ^[2] have been used to improve the resistance of metals to high-temperature oxidation and electrochemical corrosion ^[3].

Zirconium oxide is an excellent material for optical applications due to its hardness, optical transparency and high refractive index ^[4]. It is considered to be one of the most chemically and photochemically stable materials and its excellent mechanical, electrical, thermal and optical properties make it an ideal medium for photonics applications. Zirconium oxide has been widely used as an interferometry filter and for coating high power laser mirrors ^[5, 6]. Recently, thermoluminescence (TL) properties of this material were reported which showed a dependence of the main TL peak position on the crystalline structure, being centred at 135°C for the monoclinic phase and 440°C for the tetragonal phase under UV irradiation ^[7,8]. Due to its low phonon energy (about 470 cm⁻¹), Zirconia can be used for achieving higher luminescence efficiency as the number and probability of radiative transitions increase when doped with various rare earth ions ^[9]. This fact has increased the interest in developing rare-earth-doped Zirconium oxide and

dye-doped zirconia-ormosil^[10, 11] for photonics applications^[12, 13]. Interest is to dope ZrO_2 with rare earth ions to produce emission in the near-infrared range for medical applications as well as for communication purposes. Its application in the field of photonics is now well known because of its superior performance in active, Er^{3+} or dye doped waveguide and its highly efficient thermoluminescence response^[14, 15]. On the other hand, the rare-earth-doped samples presenting an emission in the visible range may find a number of applications such as active optical windows, new generation television screens and as phosphor materials.

Zirconia (ZrO_2) primarily exists in three different polymorphs with increasing temperature at ambient pressure: the monoclinic phase, from room temperature to 1175 °C; the tetragonal phase, from 1175 to 2370 °C; and the cubic phase, from 2370 to 2750 °C (melting point)^[16]. The phonon energy of the ZrO_2 host varies with the crystal phases; therefore the properties of ZrO_2 may depend strongly on the phase formation and transition. The room-temperature monoclinic phase has no practical applications since its formation during cooling from the high-temperature tetragonal phase is associated with the volume expansion, which results in crumbling of the ceramic components. On the other hand, the high-temperature ZrO_2 phases are suitable for various industrial applications such as solid electrolytes in solid oxide fuel cells^[17] and sensors,^[18] as a catalyst/catalyst support,^[19, 20] as membranes^[21] and as dispersed phase in composite materials^[22]. Hence, traditionally high-temperature ZrO_2 phases have been stabilized at room temperature by doping trivalent cations in the ZrO_2 lattice^[23]. The high-temperature tetragonal phase can also be stabilized at room temperature without doping any trivalent impurities, provided ZrO_2 is synthesized in its nanocrystalline form^[24]. So, it is now well recognized that the mechanical, electrical, chemical, as well as catalytic properties of Zirconia can be improved by using nanocrystalline instead of conventional micrometer-sized Zirconia^[25].

Tetragonal phase stabilization in nanocrystalline ZrO_2 is not a constant but may change under specific conditions, which in turn affects the stability range of the involved phases^[26, 27]. Some properties and structural parameters of the oxide are given below.

Formula	Molar mass	Appearance	Density	Melting point	Crystal structure	Space group
ZrO ₂	123.218 g/mol	White powder	6.68 g/cm ³	2715°C	Monoclinic (primitive)	P2 _{1c}

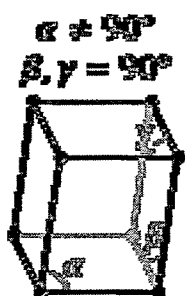


Figure 1: Monoclinic structure

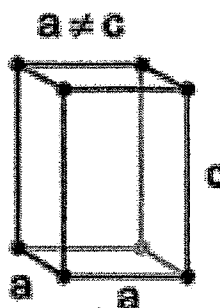


Figure 2: Tetragonal Structure

The Baddeleyite, ZrO₂ has a structure that originally was described as rather simple distortion of the fluorite arrangement ^[28]. Its symmetry is monoclinic. In this arrangement, the zirconium atoms exhibit sevenfold coordination with Zr – O distance between 2.04 and 2.26 Å. The two oxygen atoms are differently coordinated, O(1) having three Zirconium neighbours at 2.04 to 2.15 Å and O(2) having four Zirconium neighbours at 2.16 – 2.26 Å. The O – O distance is 2.52 Å. Cubic form has a fluorite arrangement. A tetragonal form contains four molecules in a prism and it is also a distorted fluorite grouping.

6.2 Synthesis of Samples

The samples of Zirconium oxide doped with rare earth activators like Europium and Terbium were synthesized by the following methods.

1. Ceramic method (Solid State synthesis)
2. Solution Combustion method
 - I. Furnace Combustion
 - II. Microwave induced combustion
3. Co-Precipitation Method

Zirconyl Nitrate Hydrate ($\text{ZrO}(\text{NO}_3)_2 \cdot \text{H}_2\text{O}$ - 99.9% purity) of Loba chemicals make, Europium Nitrate Hexa hydrate ($\text{Eu}(\text{NO}_3)_3 \cdot 6\text{H}_2\text{O}$, 99.9% purity) & Terbium Nitrate Hydrate ($\text{Tb}(\text{NO}_3)_3 \cdot x\text{H}_2\text{O}$, 99.9% purity) of Alfa Aesar and Urea (NH_2CONH_2 , 99% purity) of Qualigens, were used as the precursor materials.

For the synthesis of Zirconium dioxide by Solid State reaction method, 5 grams of Zirconyl Nitrate was mixed with Europium/Terbium as nitrates in stoichiometric proportion for a 2 mole percent incorporation. A minimum amount of water was added and the contents were mixed thoroughly by agate mortar and pestle. The resulting paste was transferred into silica crucible and heated at 1100°C for 4 hours. The obtained product was a dense cake which was crushed and grinded to fine powder with mortar and pestle. The powder was washed with acetone to remove the residual impurities like nitrate ions. The final product obtained was pure white coloured powder.

For synthesis by Furnace combustion method, 5 grams of Zirconyl Nitrate (*oxidizer*) and 2 mole percent equivalent of Europium/Terbium as nitrates was mixed with varying amounts of Urea (*fuel*) for stoichiometric (1.66), fuel rich (2.0) and fuel deficient ratios (1.32) in a 250 ml Schott Duran (Germany) Round Bottom flask. The corresponding equivalence ratio ϕ_e (discussed in Chapter 3) was calculated and found to be 1.002 for stoichiometric, 0.90 for fuel rich and 1.143 for fuel lean ratios. The amount of water added to the mixture was about 0.667 ml/gm of nitrate ^[29]. It was heated at moderate rate with stirring for 30 minutes to allow homogenous mixing of the constituents. The mixture was then introduced into a muffle furnace preheated at around 500°C . Initially the mixture starts boiling and slowly the water gets evaporated. The solution (paste) melts (boils) and undergoes dehydration followed by decomposition with the evolution of large amounts of gases (oxides of nitrogen and ammonia). The redox mixture is then auto ignited resulting in an exothermic reaction with a reddish white flame persistent for relatively longer time compared to other hosts reaching temperature above 1100°C . White fluffy cake was obtained which was voluminous, porous and foamy in nature. This cake was grinded with mortar and pestle to obtain fine powder which was then

washed with acetone to remove the residual impurities. The final product was pure white coloured fine powder.

In case of Microwave combustion synthesis, the above mentioned mixtures were taken in a 250 ml Schott Duran (Germany) round bottom flask and placed inside a modified kitchen microwave oven (discussed in Chapter 3) with output power of 850 watts and frequency of 2.45 GHz for a few minutes. During this time, the redox mixture boiled with the evolution of large amount of gas, underwent dehydration and ignited (due to internal heating) resulting in an exothermic reaction with a white flame (persistent for longer duration) releasing large amount of heat. Here also, a white cake was obtained which was voluminous, porous and foamy in nature. The powder was washed with acetone to remove the residual impurities and grinded with mortar and pestle. The final product was pure white coloured fine powder.

In Co-precipitation method, 3.249 gram of $ZrO(NO_3)_2$ was dissolved in 50 ml of alcohol to obtain 0.2 mol/liter solution. This solution was added drop wise into an alcoholic solution of 2 mol/liter ammonium hydroxide at the rate of 4 ml/minute and vigorously stirred. The temperature was maintained at 50° C. As the precipitation occurred, the final pH of the solution was greater than 9. These precipitates were filtered and washed with acetone several times to get rid of residual impurities. The precipitates were dried in a vacuum desiccator for 10-12 hours and finally dried in an oven at 100°C for 12 hrs. Zirconium Hydroxide nanoparticles were obtained. These nanoparticles were calcined at 600° C for 2 hours to obtain the Zirconium Oxide nanoparticles. The powders thus obtained were collected in glass bottles.

6.3 Characterization of Samples

These samples were characterized by X-ray diffraction (XRD). They were further investigated by Scanning electron microscopy (SEM). Their Fluorescence and UV-Visible characteristics were also studied.

X - Ray Diffraction

The XRD patterns were taken of Bruker D8 advance X-ray diffractometer. The 2θ range was taken from 25° to 80° in scan mode with step increment of 0.050° and step time 2 seconds at room temperature. The data were smoothed and then considered. The X-ray diffraction patterns of the samples are given below. Out of the total nine samples, three samples have been synthesized by furnace combustion method and other three by microwave combustion method with fuel lean, stoichiometric and fuel rich ratios respectively. One sample has been synthesized by Solid state synthesis method and another by Co-precipitation method. The XRD patterns are given in Figures Z_x 1 to Z_x 9 accordingly. The XRD of commercially available sample is also given for reference.

Reflections for sample Z1 i. e. commercially available material, show very sharp features with high intensity. Many peaks are observed. To identify the sample structure, 10 prominent peaks were considered. The peak at 2θ value of 28.206° has the highest intensity followed by peaks at 31.479° and 50.171° . d values of all the peaks match very closely with those reported in JCPDS file number 83-0944. There is an extra peak observed at 2θ value of 30.174° . No appreciable peak broadening is observed.

Reflections for sample Z2 prepared by solid state method show very sharp features with high intensity. The peak at 2θ value of 28.381° has the highest intensity followed by peaks at 31.657° and 34.377° . d values of all the peaks match very closely with those reported in JCPDS file number 83-0944. The peak broadening is minimum in this case. The extra peak observed at 2θ value of 30.174° for Z1 is absent in this sample. The rest of the peaks of sample Z2 match closely with sample Z1. The intensities of the peaks are relatively less compared to Z1.

Reflections for sample Z3 prepared by furnace combustion in fuel rich proportion show sharp features with high intensity. Eight prominent peaks were considered. The peak at 2θ value of 30.288° has the highest intensity followed by peaks at 50.458° and 59.952° . d values of all the peaks match very closely with those reported in JCPDS file number 79-1770. Some amount of peak broadening is observed here. The intensities of all the peaks are observed to be quite high compared to samples Z1 and Z2. The peaks at 2θ

value of 27.247°, 30.288°, 35.113°, 50.458°, 59.952°, 62.909° match with XRD pattern of samples Z1 and Z2.

Reflections for sample Z4 prepared by furnace combustion in stoichiometric proportion show sharp features with high intensity. The peak at 2θ value of 30.274° has the highest intensity followed by peaks at 50.422° and 59.970°. d values of all the peaks match very closely with those reported in JCPDS file number 79-1770. The amount of peak broadening is observed to be more than sample Z3. The intensities of all the peaks are observed to be quite high compared to samples Z1 and Z2 but lower than sample Z3. The peaks at 2θ value of 27.225°, 30.274°, 35.099°, 50.422°, 59.970°, 62.876° match with XRD pattern of samples Z1, Z2 and Z3.

Reflections for sample Z5 prepared by furnace combustion in fuel lean proportion also show sharp features with high intensity. Eight prominent peaks were considered. The peak at 2θ value of 30.210° has the highest intensity followed by peaks at 50.334° and 59.981°. d values of all the peaks match very closely with those reported in JCPDS file number 79-1770. The amount of peak broadening is observed to be more than samples Z1, Z2, Z3, Z4. The intensities of all the peaks are observed to be quite high compared to samples Z1 and Z2 but lower than samples Z3 and Z4. The peaks at 2θ value of 27.215°, 30.210°, 35.079°, 50.334°, 59.981°, 62.825° match with XRD pattern of samples Z1, Z2, Z3 and Z4.

XRD of Sample Z 1

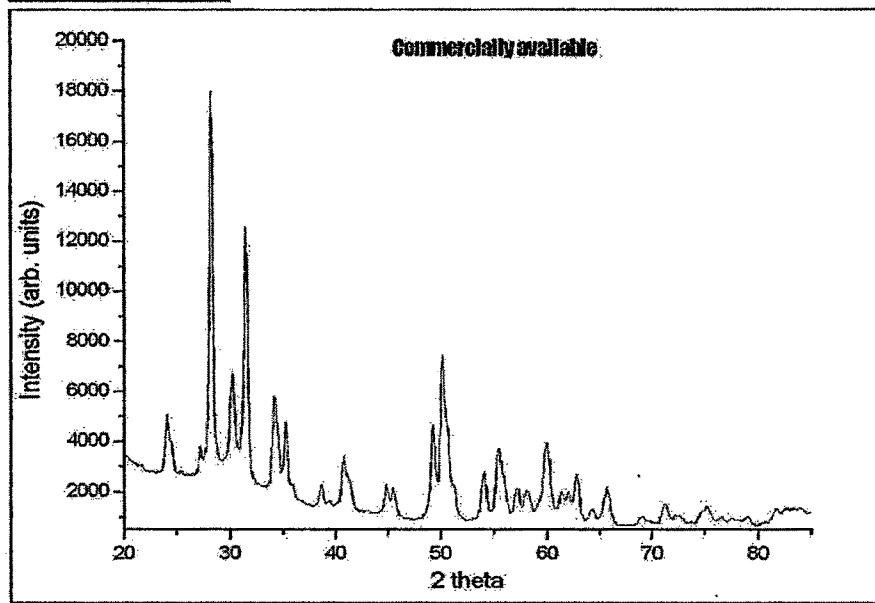


Figure Z_x 1

XRD of Sample Z 2

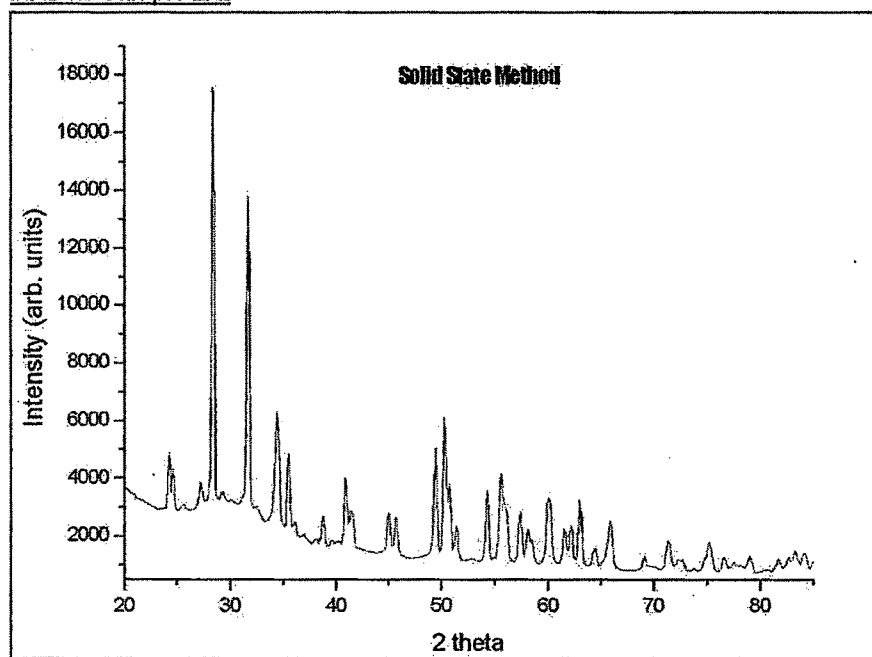
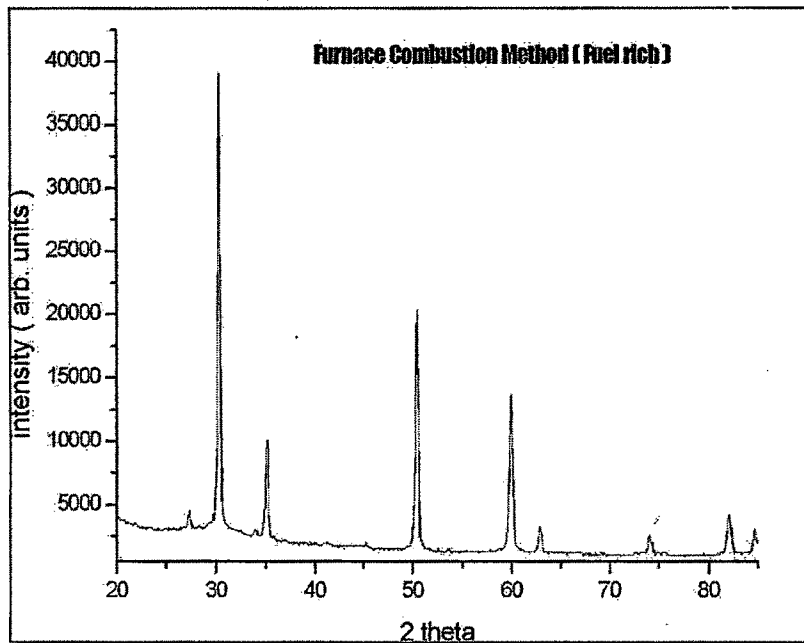
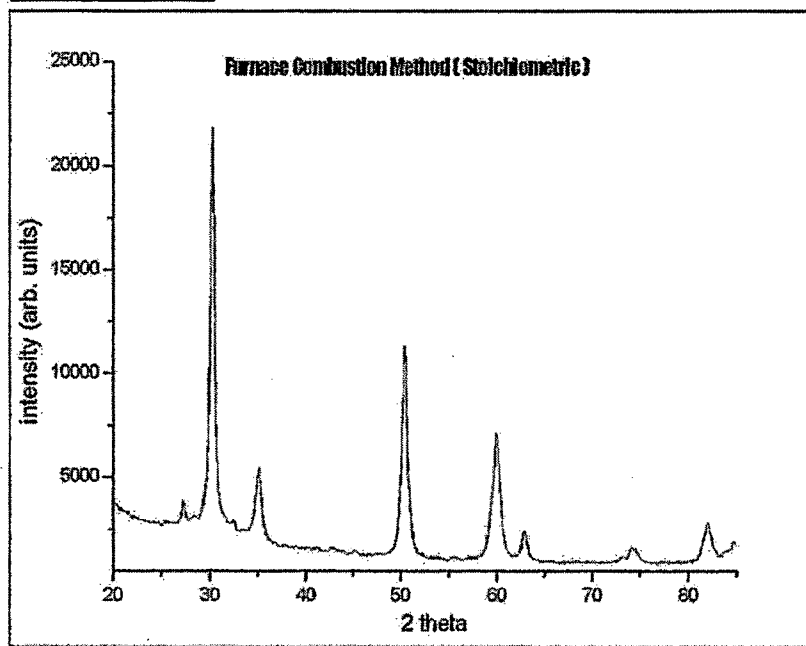


Figure Z_x 2

XRD of Sample Z 3

Figure Z_x 3

XRD of Sample Z 4

Figure Z_x 4

XRD of Sample Z 5

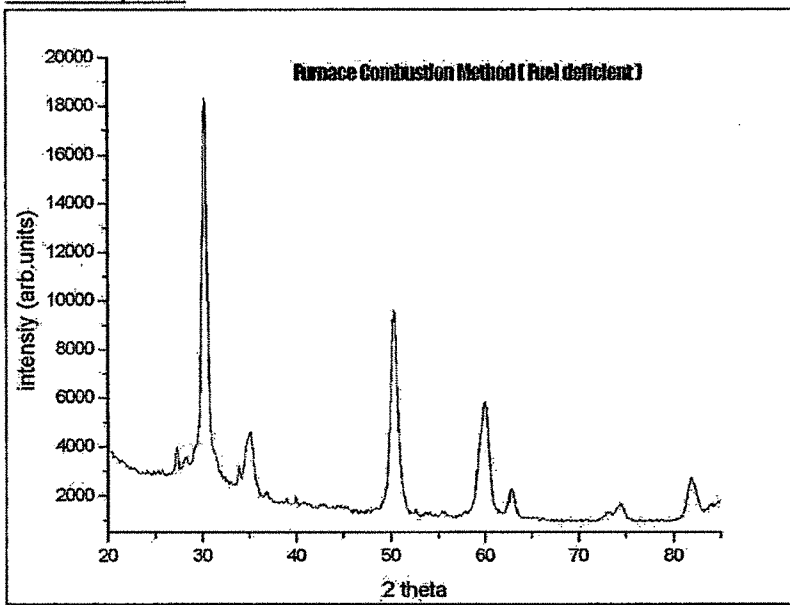


Figure Z_x 5

XRD of Sample Z 6

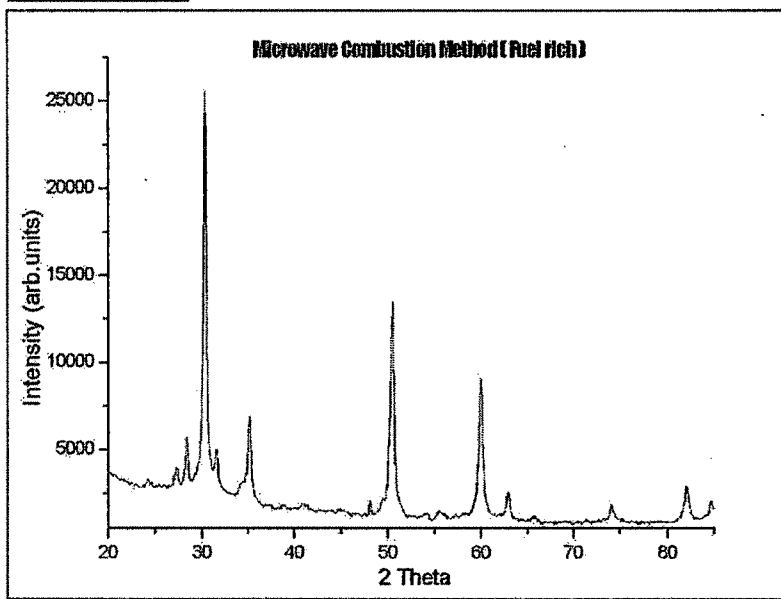
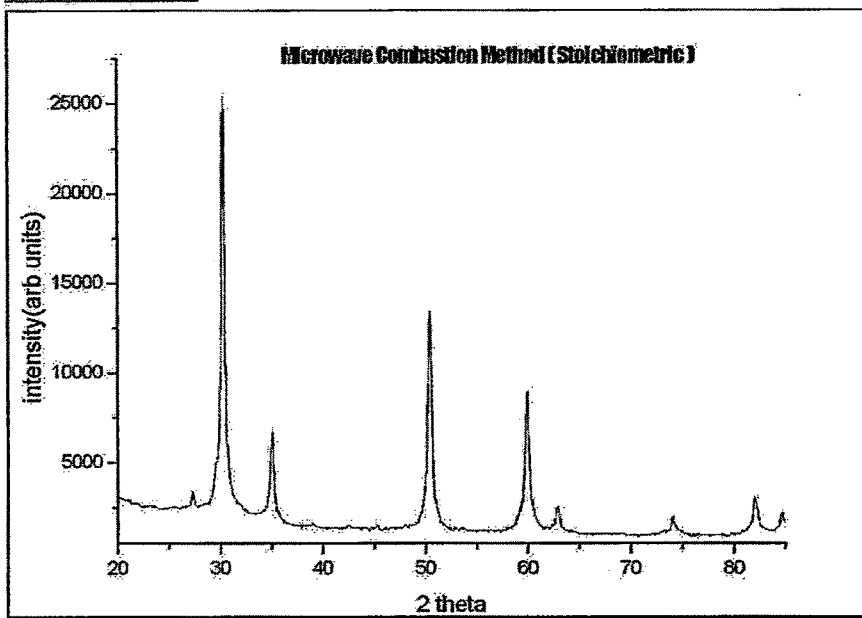
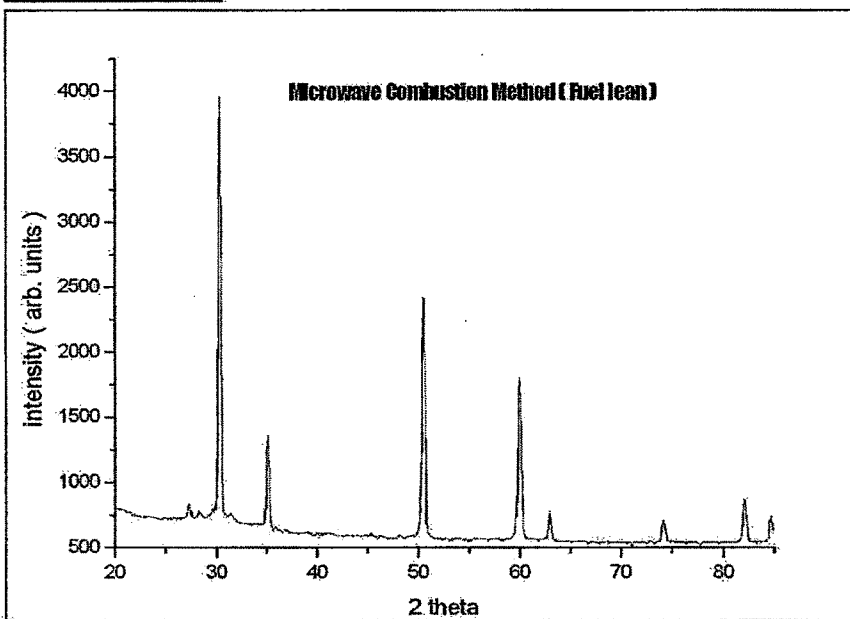
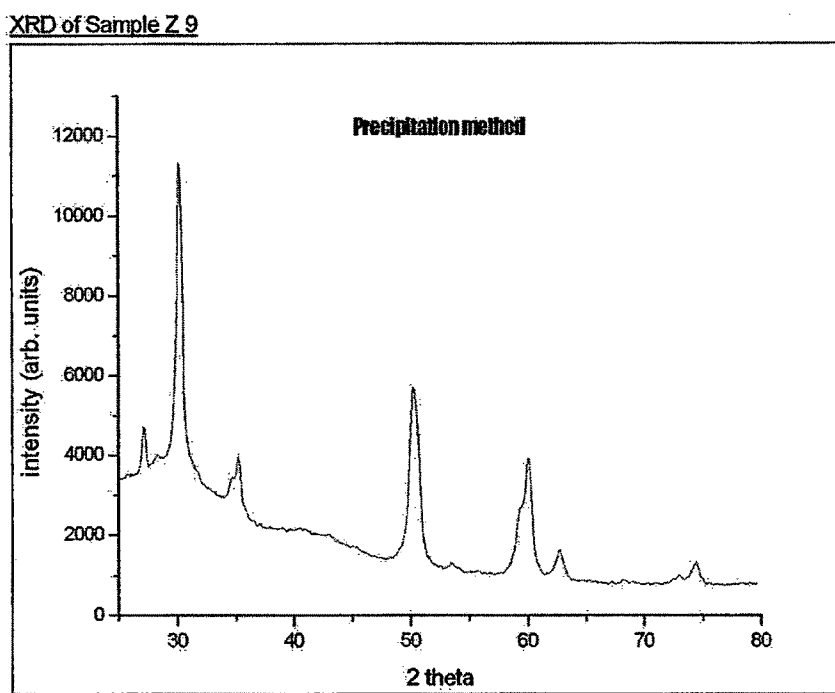


Figure Z_x 6

XRD of Sample Z 7Figure Z_x 7XRD of Sample Z 8Figure Z_x 8

Figure Z_x 9

Reflections for sample Z6 prepared by microwave combustion in fuel rich proportion also show sharp features with relatively moderate intensity. Eight prominent peaks were considered. The peak at 2θ value of 30.319° has the highest intensity followed by peaks at 50.488° and 59.988° . d values of the peaks match relatively less closely with those reported in JCPDS file number 79-1770 than the above mentioned samples. The amount of peak broadening is comparable to sample Z3 but more than samples Z1 and Z2. It is less than samples Z4 and Z5. The intensities of all the peaks are observed to be quite low compared to samples Z1, Z2, Z3, Z4, and Z5. The peaks at 2θ value of $27.253^\circ, 30.319^\circ, 35.131^\circ, 50.488^\circ, 59.988^\circ, 62.936^\circ$ match with XRD pattern of samples Z1, Z2, Z3, Z4 and Z5.

Reflections for sample Z7 prepared by microwave combustion in stoichiometric proportion also show sharp features with high intensity. The peak at 2θ value of 30.273° has the highest intensity followed by peaks at 50.434° and 59.939° . d values of all the peaks match closely with those reported in JCPDS file number 79-1770. The amount of peak broadening is comparable to sample Z3 but more than samples Z1 and

Z2. It is less than samples Z4, Z5 and Z6. The intensities of the peaks are observed to be higher than other samples except Z3. The peaks at 2θ value of $27.222^\circ, 30.273^\circ, 35.080^\circ, 50.434^\circ, 59.939^\circ, 62.885^\circ$ match with XRD pattern of samples Z1, Z2, Z3, Z4, Z5 and Z6.

Reflections for sample Z8 prepared by microwave combustion in fuel lean proportion also show sharp features with high intensity. The peak at 2θ value of 30.370° has the highest intensity followed by peaks at 50.521° and 60.022° . d values of all the peaks match closely with those reported in JCPDS file number 79-1770. The amount of peak broadening is comparable to sample Z3 but less than samples Z4, Z5, Z6 and Z7. The intensities of the peaks are observed to be higher than other samples but lower than sample Z3. The intensities are comparable to sample Z7. The peaks at 2θ value of $27.236^\circ, 30.370^\circ, 35.175^\circ, 50.521^\circ, 60.022^\circ, 62.954^\circ$ match with XRD pattern of samples Z1, Z2, Z3, Z4, Z5, Z6 and Z7.

Reflections for sample Z9 prepared by co-precipitation method also show sharp features with moderate intensity. Eight prominent peaks were considered. The peak at 2θ value of 30.209° has the highest intensity followed by peaks at 50.318° and 60.060° . d values of all the peaks match closely with those reported in JCPDS file number 79-1770. The amount of peak broadening is more than all the previous samples. The intensities of all the peaks are observed to be less compared to samples Z1, Z2, Z3, Z4, Z5, Z7, Z8 but more than sample Z6. The peaks at 2θ value of $27.172^\circ, 30.209^\circ, 35.144^\circ, 50.318^\circ, 60.060^\circ, 62.759^\circ$ match with XRD pattern of samples Z3, Z4, Z5, Z6, Z7 and Z8.

In all the samples small peaks are observed at 2θ value of 27.23° , and 28.34° . The intensity of these peaks become high in samples Z8 and Z9. In general it is found that the broadening of peaks is minimum for samples synthesized by solid state synthesis. It increases in the order; Microwave combustion, Furnace combustion, Co-precipitation. For samples synthesized by combustion synthesis method, it is found that the broadening increases in the order: Fuel deficient ratio, stoichiometric ratio and fuel rich ratio for microwave and combustion synthesis methods. Samples synthesized by furnace combustion method give higher intensity compared to samples synthesized by

microwave combustion. The d values of the respective samples are given in Table 1 as under.

JCPDS 79-1770	Z9	Z8	Z7	Z6	Z5	Z4	Z3	Z2	Z1	JCPDS 83-0944
3.242	3.27925	3.27142	3.27286	3.26983	3.27427	3.27247	3.27074	3.14337	3.16143	3.1598
2.965	2.95609	2.94147	2.95063	2.94607	2.95654	2.94985	2.94860	2.82443	2.84041	2.8375
2.4555	2.55146	2.54936	2.55604	2.55217	2.55457	2.55513	2.55389	2.60616	2.62101	2.6213
1.8068	1.81191	1.80544	1.80789	1.80616	1.81131	1.80851	1.80724	2.52717	2.54244	2.538
1.543	1.53921	1.54019	1.54191	1.54072	1.54137	1.54115	1.54168	1.84225	1.84663	1.8459
1.4761	1.47934	1.47534	1.47651	1.47542	1.47808	1.47675	1.47621	1.68890	1.69452	1.693
1.2776	1.27366	1.27775	1.27862	1.27811	1.27341	1.27779	1.27854	1.60554	1.60964	1.6083
1.1733		1.17308	1.17376	1.17325	1.17495	1.17405	1.17353	1.53940	1.54108	1.5429
								1.47405	1.47822	1.4764
								1.41695	1.42050	1.424

Table 1: d values of samples

All the X ray reflection peaks of the XRD patterns given from figures Z_x 3 to Z_x 9 of samples synthesized by combustion method and precipitation method could be indexed exactly with the reported values in the JCPDS file 79-1770 of Zirconium oxide and confirm the formation of Tetragonal structure with the space group P4₂/nmc. The peaks from XRD patterns of Zirconium oxide synthesized by solid state method and commercially available samples given in figure Z_x 1 and Z_x 2 could be indexed with reported values in JCPDS file 83-0944 of Zirconium oxide and confirm the formation of Monoclinic structure with space group P2₁/c. Good amount of broadening in the peaks is observed for samples synthesized by Combustion method and Co- precipitation method compared to sample synthesized by solid state and commercially available sample, which are basically bulk samples. The calculated d values for the respective peaks along with the variation in their intensities pattern is shown in figure Z_x 10 and Z_x

11. This pattern is consistent with the ones given in the relevant JCPDS files, although the intensities of the peaks in JCPDS files is low.

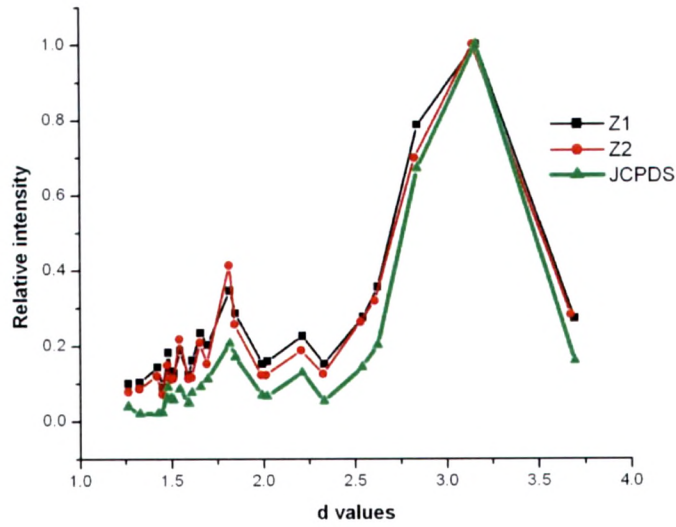


Figure Z_x 10

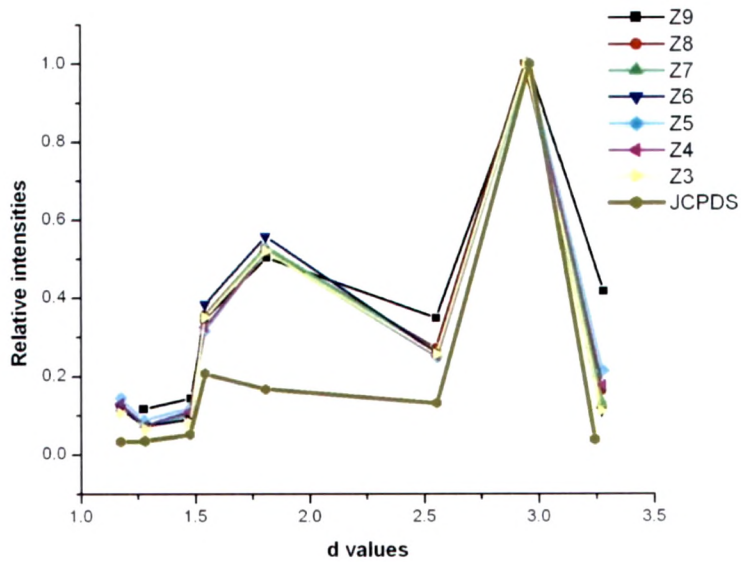


Figure Z_x 11

In figure Z_x 10, the black and red lines representing the intensity patterns of the samples Z1 and Z2 match precisely with the green line giving the JCPDS intensity

patterns. The d values are also a perfect match. This confirms the monoclinic structure of the samples.

The intensity patterns of rest of the prepared samples from Z3 to Z9 in Fig. Z_x 11 are also a faithful representation of the JCPDS intensity pattern for tetragonal structure, except for the peak corresponding to the d value of around 1.8 °A.

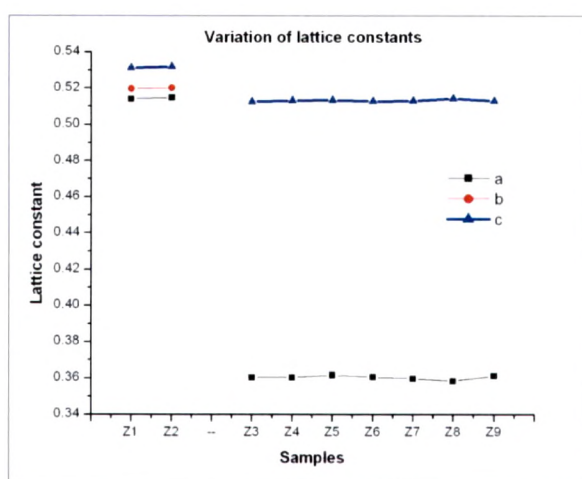
The samples Z1 and Z2 are bulk samples either taken off the shelf or made by solid state synthesis by heating up to about 1100 °C, while the rest of them are either nano crystallites or nano particles, prepared by combustion or precipitation methods. The above results are in line with the reported work mentioned earlier, which suggests that up to 1175 °C, the material remains in monoclinic phase and after that it attains tetragonal structure. This confirms that the temperatures attained during the combustion process are well beyond 1175 °C. Thus, the combustion route is a convenient short cut for producing tetragonal Zirconia. Interestingly, the co-precipitation method also yields tetragonal structure. Since the process does not involve any high temperature mechanism, the reason for this can be attributed to the smaller particle size and the subsequent surface effects. The structural parameters like lattice constant and lattice volume for the monoclinic and tetragonal phases are given in Tables 2 & 3 respectively.

Parameters for Planes (101) and (112) of ZrO ₂				
Sample	d spacing nm	Lattice constant a nm	Lattice constant c nm	Volume = a^2c nm
Z3	2.94860	0.36049	0.51251	0.066602
Z4	2.94985	0.36049	0.51319	0.066691
Z5	2.95601	0.36156	0.51334	0.067107
Z6	2.94147	0.36068	0.51269	0.066696
Z7	2.94607	0.35980	0.51292	0.066401
Z8	2.95063	0.35849	0.51420	0.066082
Z9	2.95609	0.36137	0.51292	0.066981

Table 3: Lattice constants and cell volume for Tetragonal ZrO₂

Parameters for Planes (1 ⁻ 11) and (111) of ZrO ₂						
Sample	d spacing nm	Lattice constant a nm	Lattice constant b nm	Lattice constant c nm	Lattice constant β°	Volume
Z1	0.3142	0.5139	0.5197	0.5311	99.211	0.14001
Z2	0.3161	0.5147	0.5201	0.5318	99.213	0.14052

Table 2: Lattice constants and cell volume for Monoclinic ZrO₂



The variation in the lattice parameters for different samples is presented in the figure above. The sections for the samples Z1, Z2 (monoclinic phase) is distinctly different from the other samples (tetragonal phase). For the former, there are three crystal parameters a, b & c while for the later there are only two. The lines are almost straight, indicating the consistency of structural parameters for different methods of synthesis.

The average crystallite sizes of all the samples have been calculated using Scherer equation. There is always some amount of strain present in the crystals as their size decreases. Crystal sizes without strain are calculated by graphical method, as discussed

in Chapter 2. The plots are given below along with a typical calculation for the graphical method in Table 4.

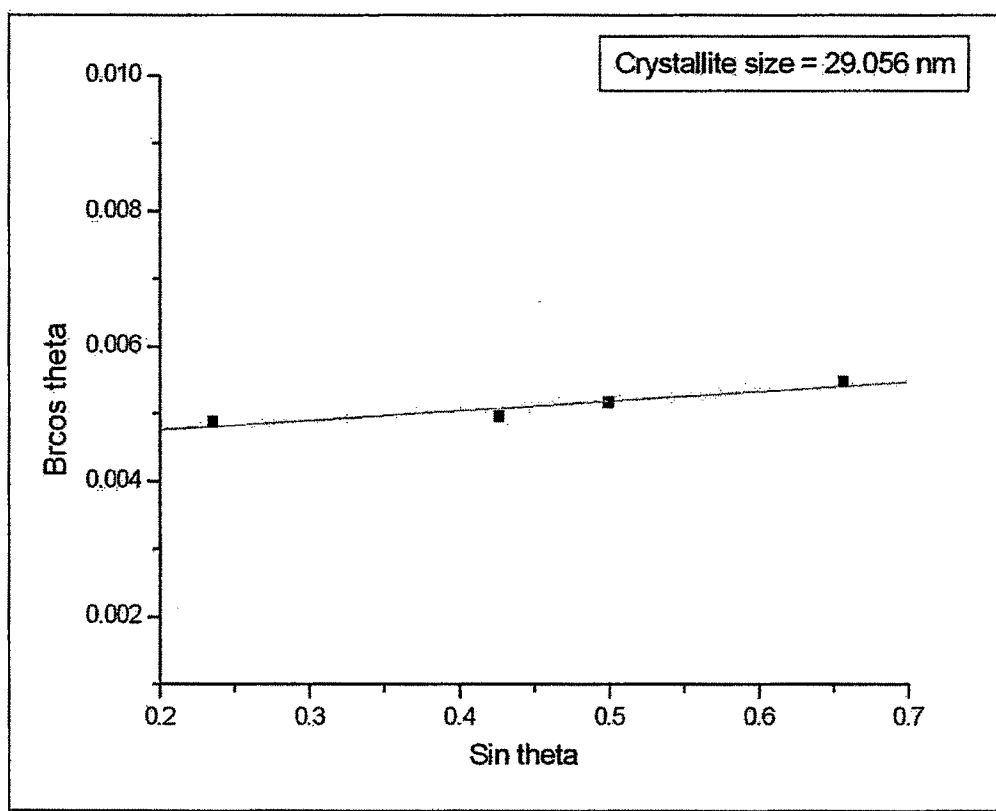
2 θ values	FWHM	Silicon 2 θ values	Silicon FWHM	B_i^2	B_o^2	$B_i = \sqrt{B_o^2 - B_i^2}$	$\sin \theta$	$B_i \times \cos \theta$
30.011	0.351	28.370	0.1145	3.993×10^{-6}	0.00003753	0.005791	0.258912	0.005594
44.799	0.339	47.238	0.1096	3.659×10^{-6}	0.00003501	0.005599	0.381062	0.005176
53.932	0.370	56.060	0.1076	3.526×10^{-6}	0.00004170	0.006179	0.453462	0.005507
71.258	0.466	69.078	0.1135	3.924×10^{-6}	0.00006615	0.007888	0.582534	0.006412

Table 4: Data for determination of crystallite size by graphical method for a typical sample (prepared by Microwave method)

Sample Z3

Crystallite Size by Scherrer Formula

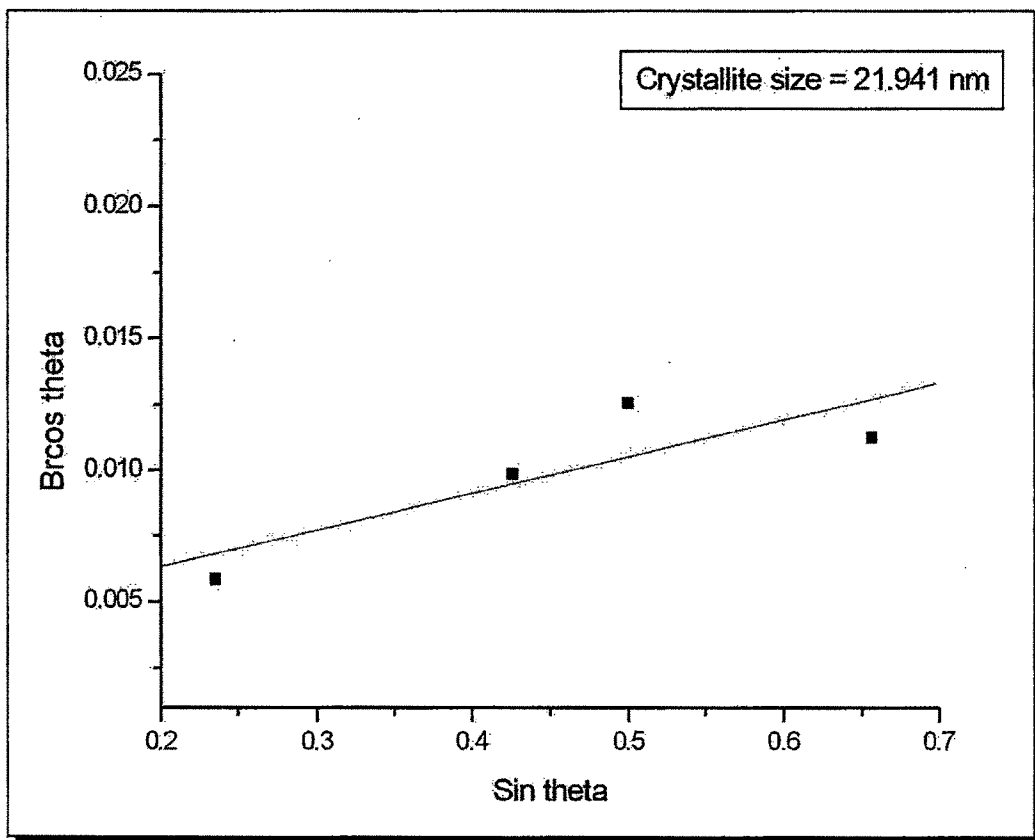
d values (°A)	Crystallite Size (nm)
3.27074	24.9051
2.94860	27.3864
2.55389	26.4827
1.80724	21.5805
1.54168	19.1684
1.47621	18.8243
1.27854	16.6871
1.17353	13.9391
Average Crystallite Size	21.122



Sample Z4

Crystallite Size by Scherrer Formula

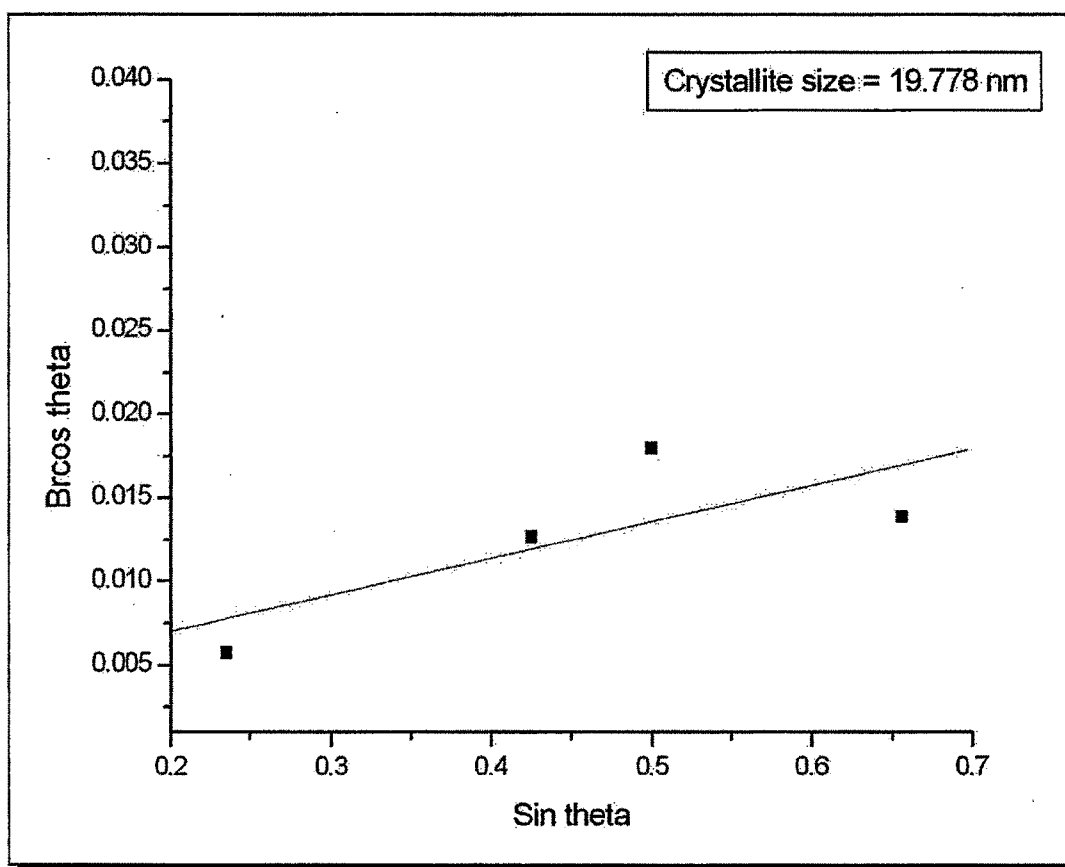
d values (°A)	Crystallite Size (nm)
3.27247	21.2113
2.94985	15.7787
2.55513	12.1578
1.80851	11.3365
1.54115	8.211
1.47675	11.5075
1.17405	6.96275
Average Crystallite Size	12.452



Sample Z5

Crystallite Size by Scherrer Formula

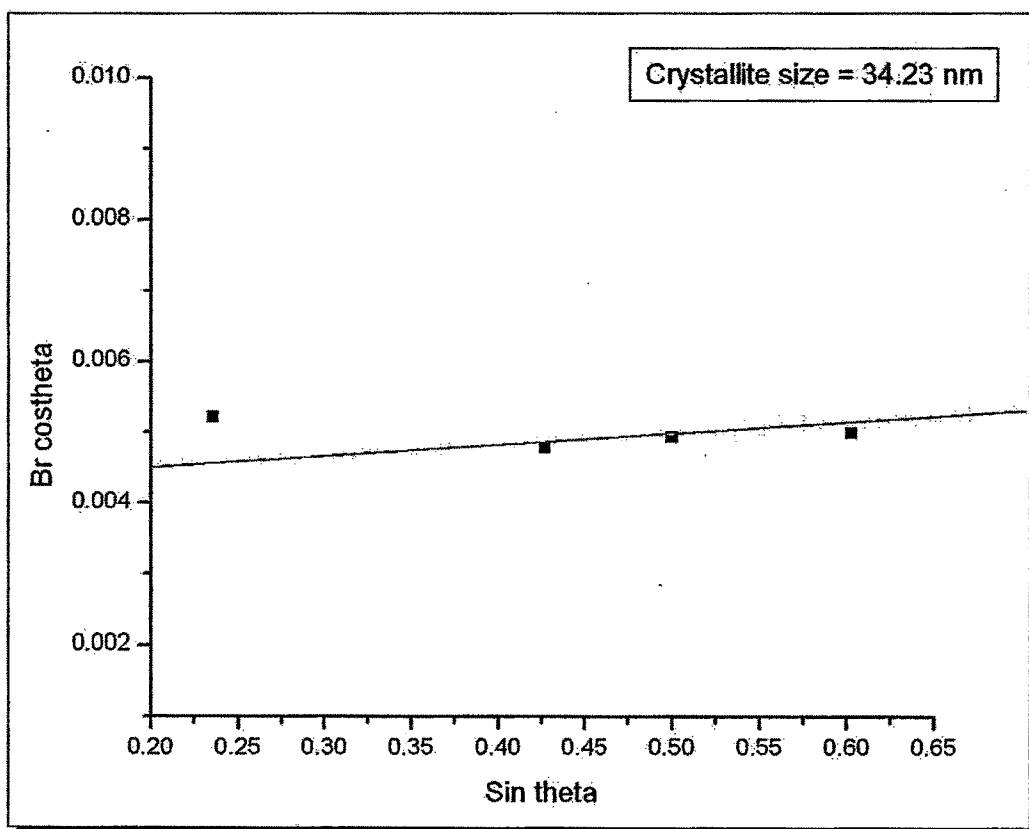
d values ($^{\circ}\text{A}$)	Crystallite Size (nm)
3.27427	21.6277
2.95654	12.677
2.55457	8.10135
1.81131	8.89848
1.54137	5.76734
1.47808	9.6578
1.17495	5.67547
Average Crystallite Size	10.344 nm



Sample Z6

Crystallite Size by Scherrer Formula

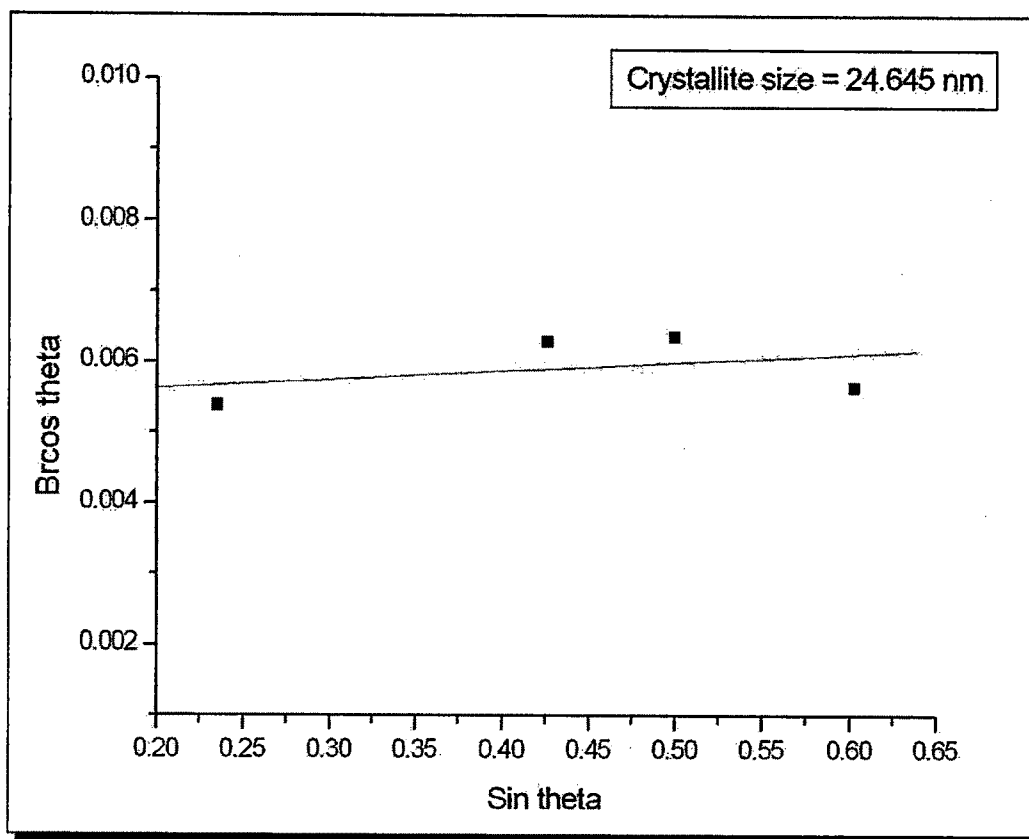
d values (°A)	Crystallite Size (nm)
3.26983	23.538
2.94607	26.5316
2.55217	25.7608
1.80616	22.315
1.54072	20.0006
1.47542	20.166
1.27811	16.905
1.17325	14.9433
Average Crystallite Size	21.27



Sample Z7

Crystallite Size by Scherrer Formula

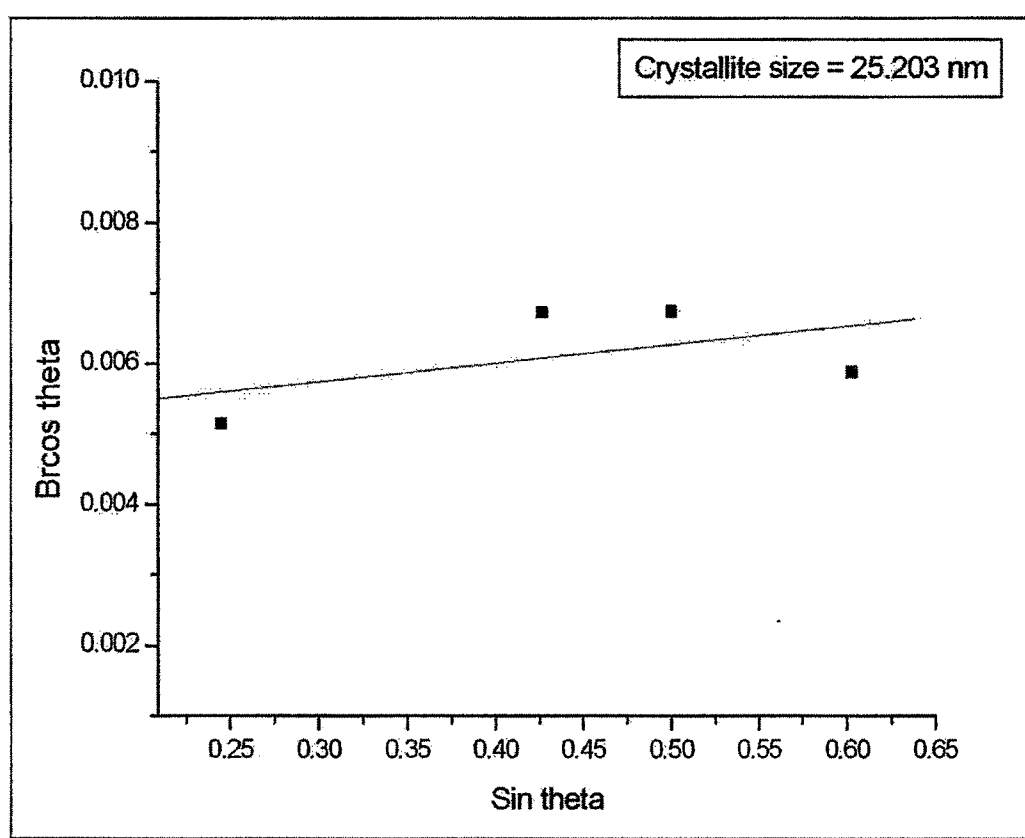
d values (°A)	Crystallite Size (nm)
3.27286	22.9109
2.95063	20.8382
2.55604	21.0995
1.80789	17.402
1.54191	15.8569
1.47651	17.1152
1.27862	15.1349
1.17376	11.7309
Average Crystallite Size	17.961



Sample Z8

Crystallite Size by Scherrer Formula

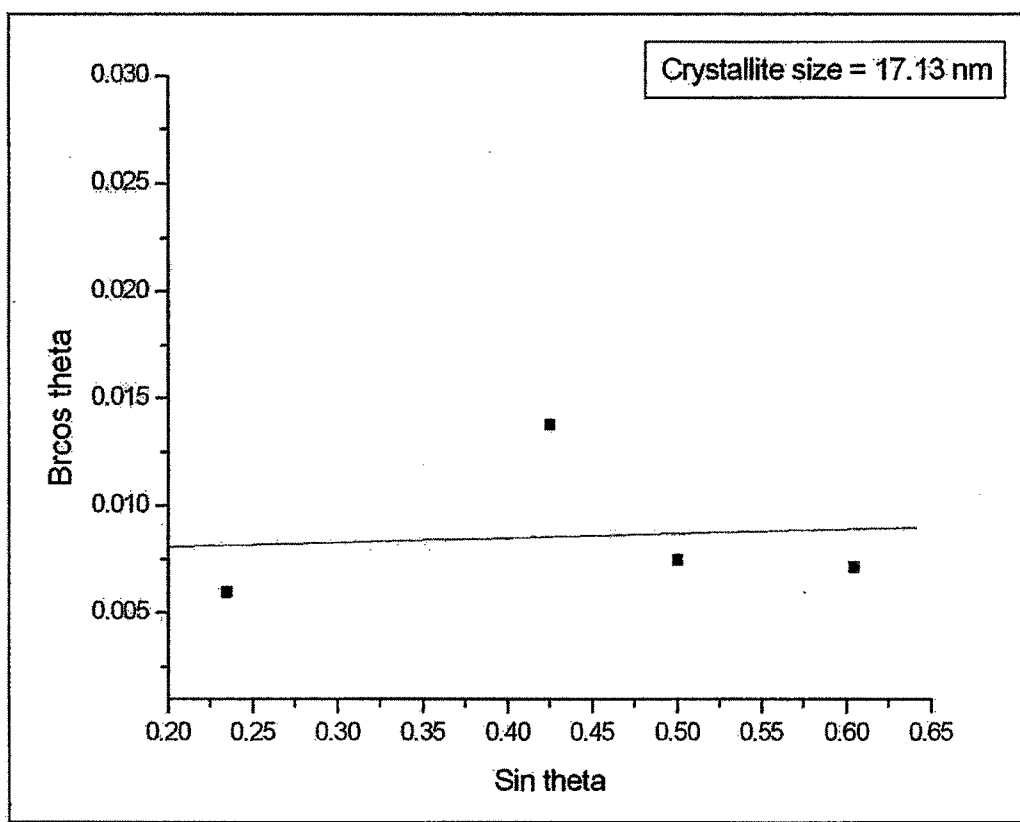
d values (°A)	Crystallite Size (nm)
3.27142	20.0019
3.14601	23.6993
2.94147	22.5492
2.54936	21.1529
1.80544	16.3283
1.54019	14.987
1.47534	16.1697
1.27775	14.5386
1.17308	11.9841
Average Crystallite Size	17.735



Sample Z9

Crystallite Size by Scherrer Formula

d values (°A)	Crystallite Size (nm)
3.27925	20.8697
2.95609	16.0118
2.55146	20.2497
1.81191	8.17095
1.53921	13.6192
1.47934	12.7245
1.27366	12.0505
Average Crystallite Size	14.814



The reaction between Zirconyl nitrate ($\text{ZrO}(\text{NO}_3)_2 \cdot 6\text{H}_2\text{O}$) and urea is highly exothermic and self propagating in nature. It is given by;



The reaction becomes vigorous with large amount of gases released. 7.6 moles of gases are released per mole of ZrO_2 formed when the fuel and oxidizer are mixed stoichiometrically. Thermochemical calculations reveal that the heat of combustion of Zirconyl nitrate redox mixtures is quite high ^[30]. Highest flame temperature is attained in stoichiometric ratio compared to fuel lean and fuel rich ratios.

As discussed earlier, a polymeric gel is formed between Zirconyl nitrate and urea mixtures which decompose to give large amount of gases. There is persistent white flame observed for almost 15 seconds in this case which may be due to reaction between oxides of nitrogen and ammonia and cyanic acid.

As discussed above, the sample synthesized by solid state method gives monoclinic structure whereas samples synthesized by combustion and co – precipitation methods give tetragonal structure. A strain free pristine bulk Zirconium dioxide is monoclinic at room temperature but undergoes a reversible martensitic phase transformation at about 1175°C to a tetragonal structure at ambient pressure ^[31]. Garvie ^[32] proposed that the tetragonal form has a lower surface free energy than the monoclinic form and the transformation temperature from monoclinic to tetragonal form decreases as the particle size decreases ^[33]. There exists a critical particle size at which high temperature tetragonal phase can be stabilized at temperatures below its normal transformation temperature down to the room temperature. Thermodynamic consideration shows that for a strain-free, isolated ZrO_2 nanocrystal, the critical nanosize for the monoclinic-to-tetragonal phase transformation, at room temperature, is 10 nm ^[34, 35]. Thus, the tetragonal structure, which provides lower surface energy gets stabilized below 10 nm particle size.

The surface energies of the ZrO_2 nanoparticles are modified as the nanoparticles synthesized under specific conditions are not single isolated particles but form

aggregates. Taking this factor into consideration, the change in surface free energy (better called interfacial energy) results into a modified critical particle size of 33 nm^[36] for the tetragonal phase stabilization of a typical aggregate. Thus, the critical size increases from 10 to 33 nm when the single, isolated ZrO₂ nanocrystals become elements of an aggregated particle. Hence, the critical size for the tetragonal-to-monoclinic phase transformation is larger when the ZrO₂ nanocrystals form aggregates than that when they exist as isolated, single, near-spherical nanocrystals. In the present investigation, ZrO₂ nanoparticles of size 14-21 nm, forming aggregates in the as-synthesized condition, crystallize into tetragonal structure (and do not transform into monoclinic structure) since their size is below the critical nanosize of 33 nm required for the tetragonal- to-monoclinic phase transformation in an aggregated condition^[37]. The crystal size of Zirconia synthesized by solid state synthesis method and commercially available samples are above the critical nanosize of 33 nm so they form monoclinic phases.

In general, for the combustion synthesis process of Zirconia, it is observed that the average crystallite size increases for samples with fuel lean ratio to stoichiometric ratio to fuel rich ratio in the same order. This is unlike the case of Ceria.

One of the major difference that was observed during the combustion synthesis between Ceria and Zirconia is that the reaction in case of the later persisted for a longer period of time with a consistent white flame, suggesting production of higher temperatures. The duration of reaction was observed to have increased with increase in the amount of fuel.

The particle size is likely to be a result of interplay between the two major competing events namely high flame temperature and evolution of large amount of gases takes place during combustion process. The former leads to more heat while the later dissipates it. The flame temperature being higher, plays a dominant role here, as it affects the formation of crystallites more profoundly than the effect due to the evolution of large amount of gases. For samples synthesized by fuel lean ratio, the

combustion process gets over in a very short period of time with almost no flame but evolution of large amount of gases, thus decreasing the temperature. Higher temperature results in more agglomeration and higher crystallite size.

In the microwave heating (discussed in Chapter 4 & 5) process, the heat is generated internally within the material instead of originating from external sources, and hence there is an inverse heating profile. The heating is very rapid as the material is heated by energy conversion rather than by energy transfer, which occurs in conventional techniques. So, one should expect that the crystals synthesized by microwave combustion method should be smaller than crystals synthesized by conventional furnace combustion method. In the case of combustion of Zirconyl nitrate - urea mixtures to give ZrO_2 , contrary effect is observed i.e. the crystals synthesized are larger for microwave combustion method than furnace combustion method. This may be due to marked difference in the decomposition/combustion behavior of the precursors i.e. Zirconium precursors burn/decompose with swelling initially and there is a persistent flame observed for longer durations in microwave combustion method, which may be due to internal heating ^[38, 39]. The flame persisted for longer durations in microwave combustion process than furnace combustion process. It may be possible that Zirconium nitrate absorbs microwaves very strongly and the internal heating process may be quite intense than furnace combustion. The exact reason still needs to be investigated further.

The average crystallite sizes are found to be smallest for samples synthesized by Co – precipitation method. This is because the heat available for the crystal growth is minimal and the agglomeration is also minimum as described in Chapter 4 for Ceria.

Scanning Electron Microscopy

Scanning electron microscopy (SEM) was done for samples synthesized by combustion (microwave and furnace) method with stoichiometric ratio, co-precipitation and solid state synthesis method. SEM was done of JEOL make JSM 5610 LV Scanning Electron Microscope.

The micrograph of sample prepared by solid state synthesis is given in figure Z_s 1. The SEM micrograph was taken with accelerating voltage of 15 KV and magnification of 10,000. The image was formed by secondary electrons signal. The particles are coarse and highly agglomerated. The particles are in irregular shape with rough edges. The grain growth is highly exaggerated. The agglomeration is due to the heat available for long time which causes the crystal to grow larger and agglomerate. Size distribution is very large. The structure is observed to be pore free.

Scanning electron micrograph of sample prepared by furnace combustion in stoichiometric ratio is given in figure Z_s 2. The SEM micrograph was taken with accelerating voltage of 15 KV and magnification of 2700. The particles are hard in nature. They are irregular in shape. The extent of agglomeration is higher. The particles have sharp edges and the growth is highly non uniform. The porosity is observed to be less.

For sample prepared by microwave combustion in stoichiometric ratio, the micrograph is given in figure Z_s 3. The SEM micrograph was taken with accelerating voltage of 15 KV and magnification of 1100. The particles are hard in nature. They are irregular in shape. The extent of agglomeration is higher. The particles have sharp edges and the growth is highly non uniform. The porosity is observed to be less. Rod shaped particles are also observed.

The SEM micrograph of powders prepared by co-precipitation method is given in figure Z_s 4. The SEM micrograph was taken with accelerating voltage of 15 KV and

magnification of 10,000. The microstructure is observed to be fine grained. The shape of the particles is round and uniform with size of about 150 to 200 nm. The agglomeration is quite less. The image reveals uniform and fine grain growth of particles.

There is a good amount of agglomeration seen in the structures which may be attributed to the fineness of the particles. Due to high surface area/volume ratio, the surface effects come into play which may be the cause of the agglomeration. Flame temperature plays a dominant role for samples prepared by microwave combustion as the product is hard agglomerate, not foamy and less porous in nature.

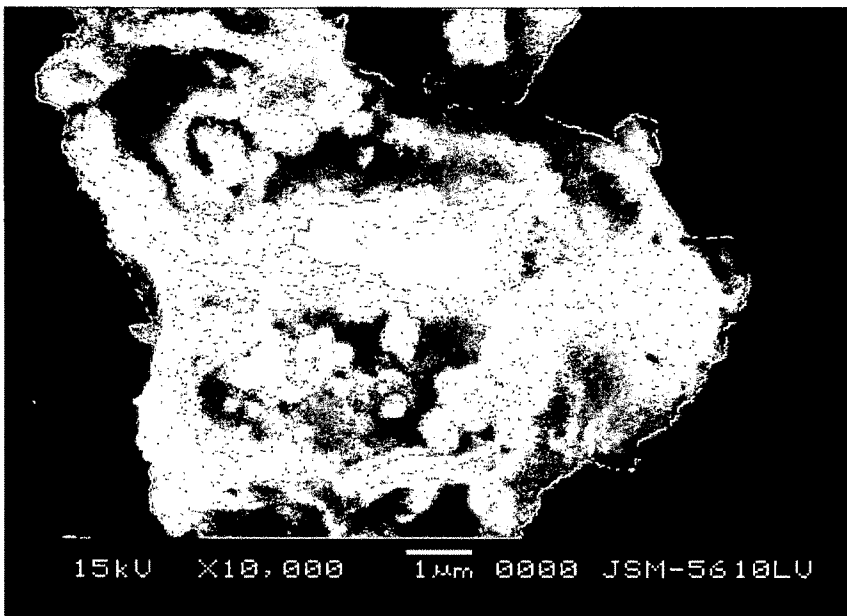


Figure Z₅ 1 Scanning Electron Micrograph of ZrO₂ synthesized by Solid State Synthesis

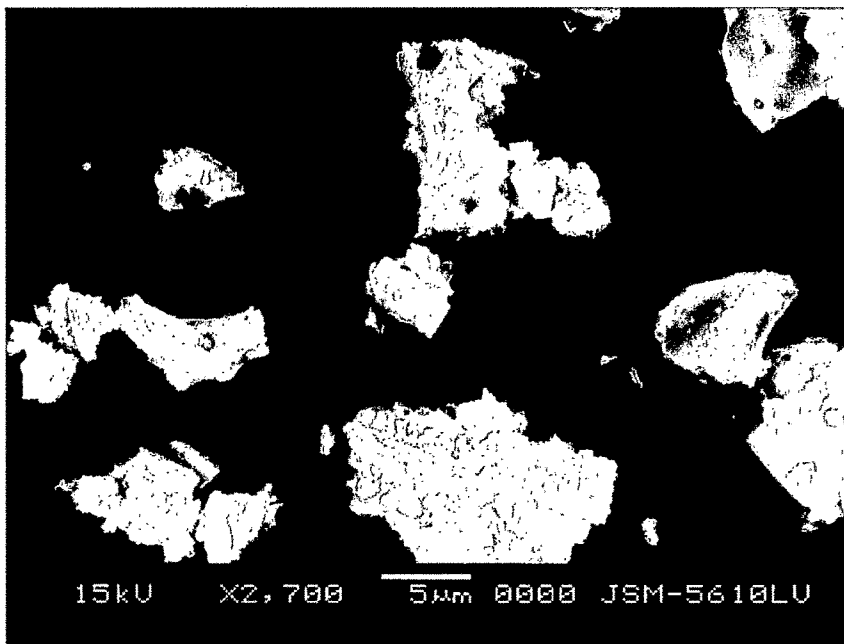


Figure Z₅ 2 Scanning Electron Micrograph of ZrO₂ synthesized by Furnace Combustion

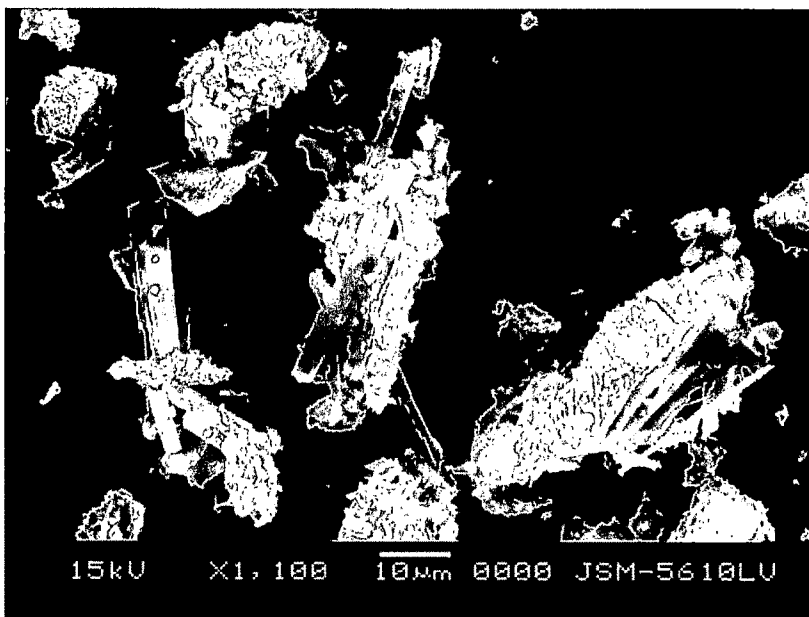


Figure Z₅ 3 Scanning Electron Micrograph of Stoichiometric ZrO₂ synthesized by Microwave Combustion

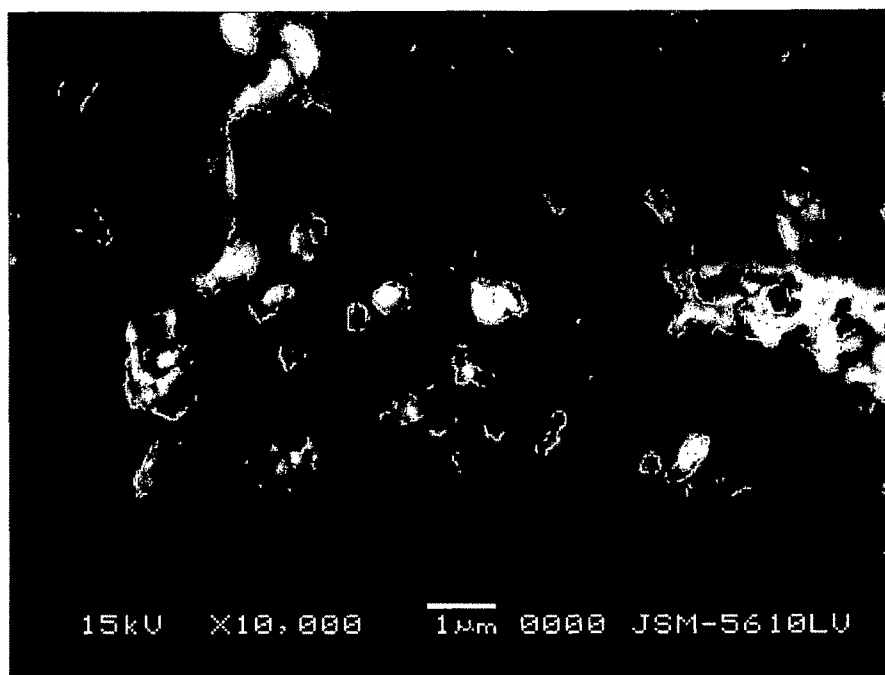


Figure Z₅ 4 Scanning Electron Micrograph of Stoichiometric ZrO₂ synthesized by Co-precipitation

Fluorescence Characteristics

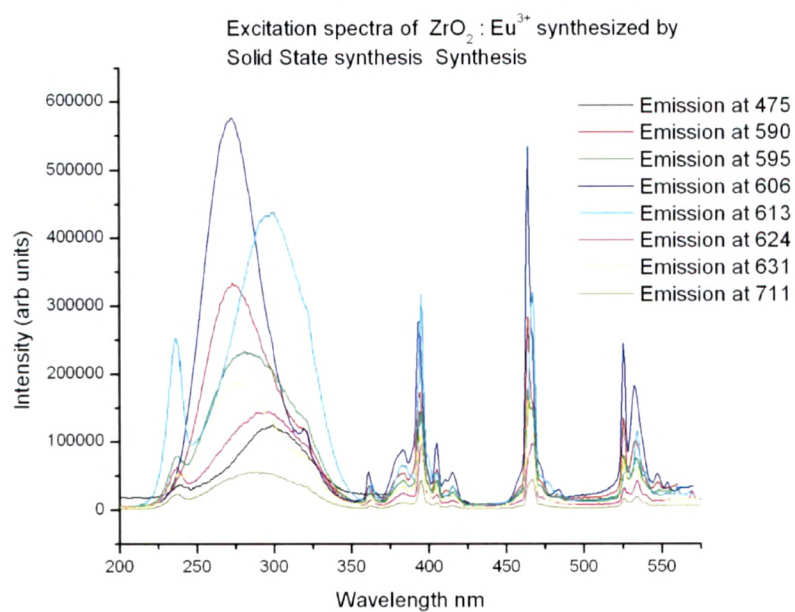
The fluorescence characteristics of the samples were recorded on a *Fluoromax 4* instrument of *Horiba Jobin Yvon* make, USA. Equal amount of samples were taken in each case. The slit width for the excitation as well as emission monochromators was fixed at 1 nm to ensure optimization and uniformity. The integration time was kept at 0.1 second.

To begin with, a random check was carried out for the emission lines. These emission lines were then used to get the exact excitation features. The reported emission spectra were taken for these precise excitation wavelengths. Thereafter, the excitation spectra were recorded for the obtained emission lines. The results are as under.

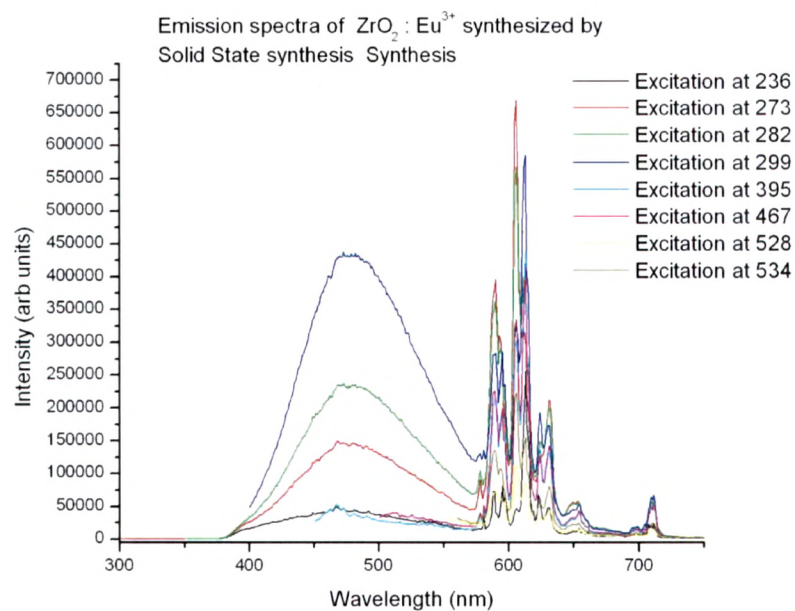
ZrO₂: Eu³⁺

The emission and excitation spectra of the samples carry simplicity as well as complexity in good proportions. The overall emission characteristics are better than the other material studied here.

The simplicity of the spectra is borne out by the consistency of the emission and excitation peaks in terms of their spectral positions. All the samples have narrow band emission peaks at the same wavelengths i.e. 590, 607, 632, 652 and 713 nm. An additional peak is seen only in the sample Z2 at 477 nm as a broad band feature. Since Z2 is the only sample with monoclinic structure, this emission can be attributed to the same. The other samples, all of whom have tetragonal structure do not show this peak. The same consistency is visible in the excitation features too. All the samples have narrow band excitation peaks at the same wavelengths i.e. 395, 464, 526 and 533 nm. The exception here is the broad band feature, whose peak spectral position shifts between 247 and 299 nm. The higher end i.e. 299 nm is observed for the sample Z2, which is a bulk sample while the lowest i.e. 247 nm is for sample Z9, which consists of nano particles. For the rest of the samples prepared by combustion methods, the variation in peak wavelength of the broad band is in a limited range. The broad band excitation features of the sample Z2 have further complexities.



ZEF1a



ZEF1b

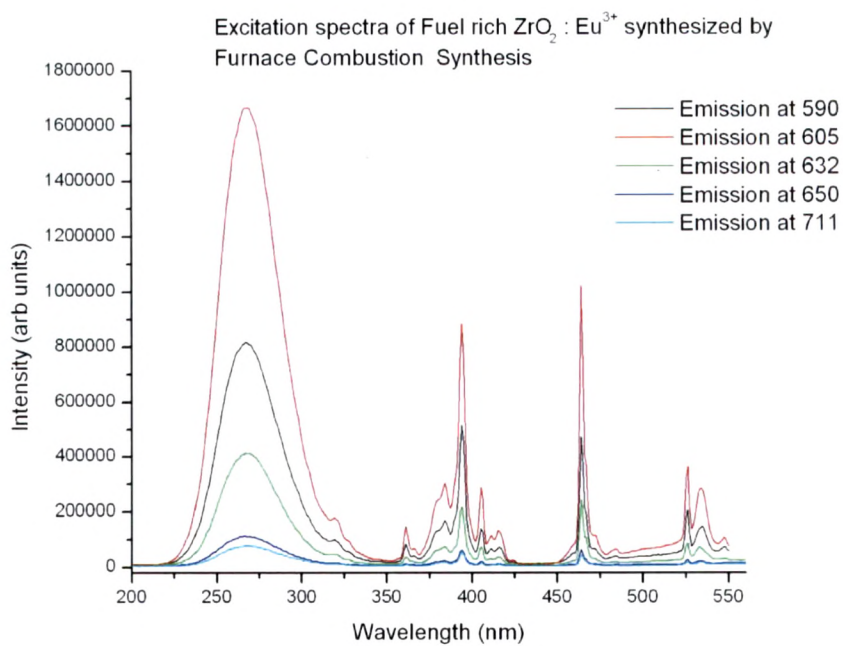


Figure: ZEF2a

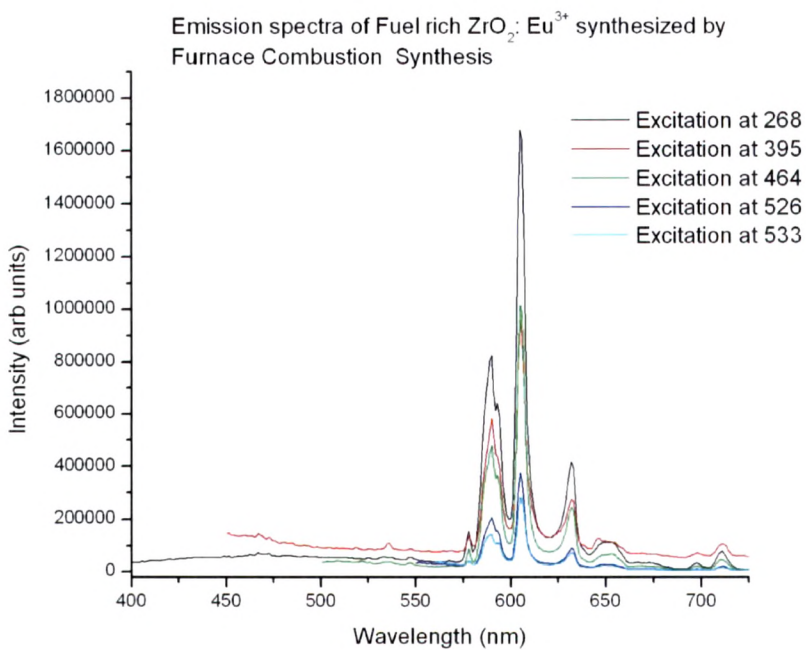


Figure: ZEF2b

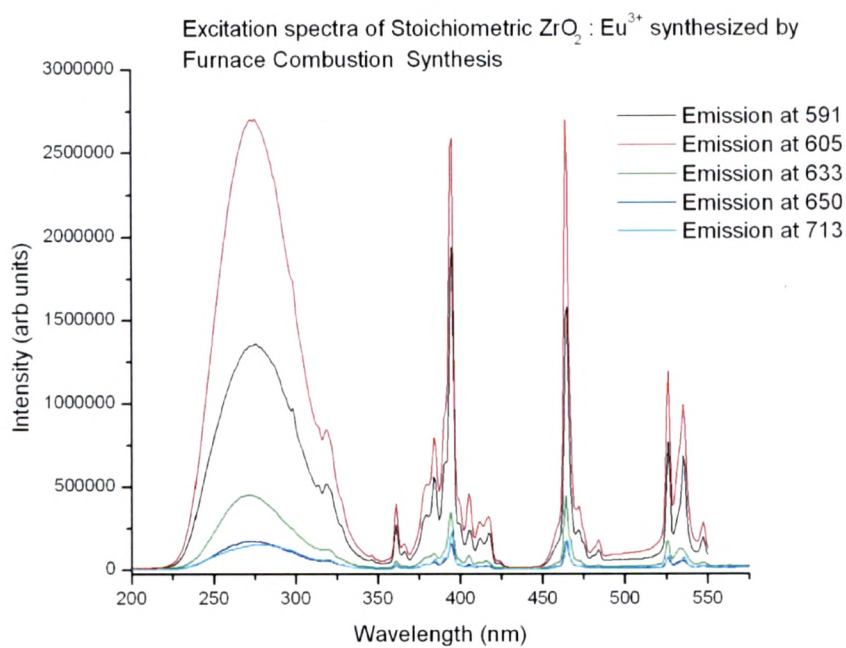


Figure: ZEF3a

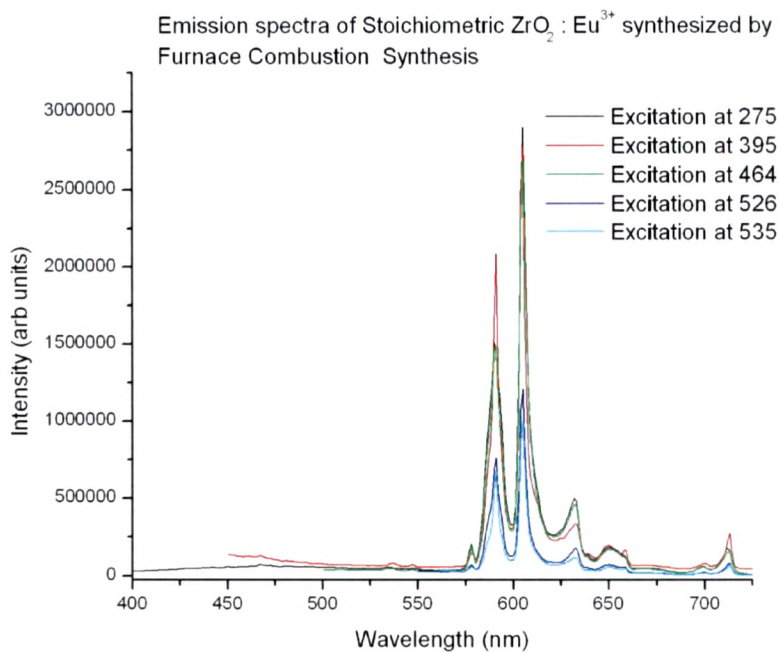


Figure: ZEF3b

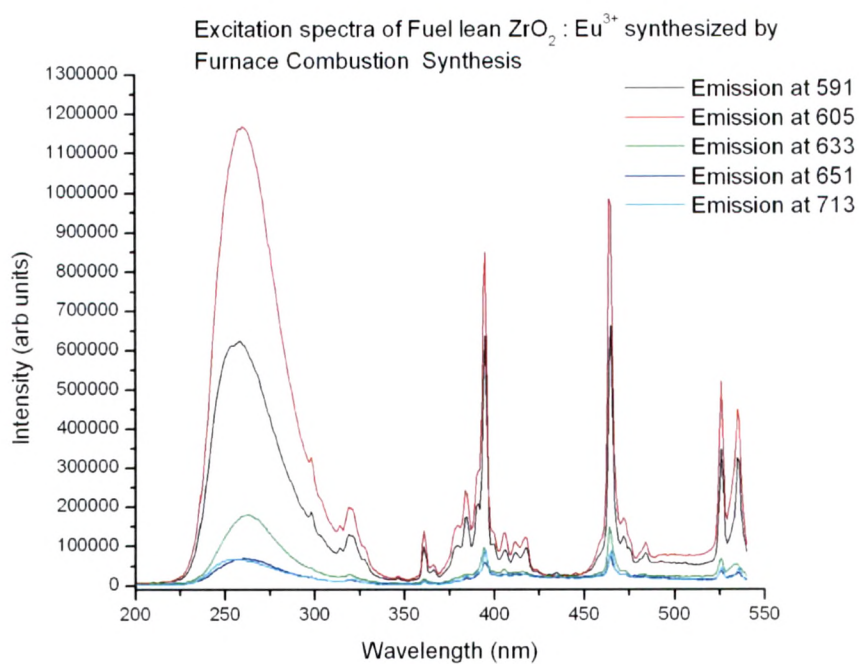


Figure: ZEF4a

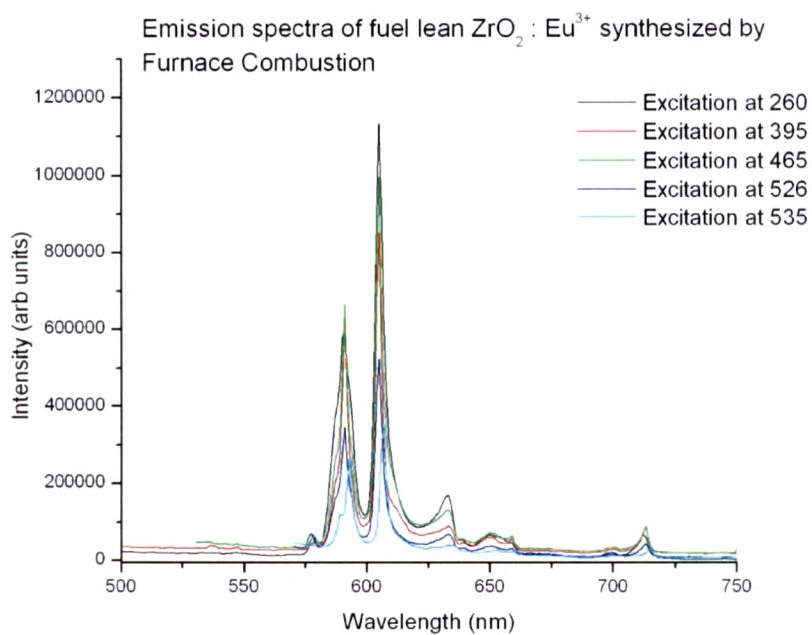


Figure: ZEF4b

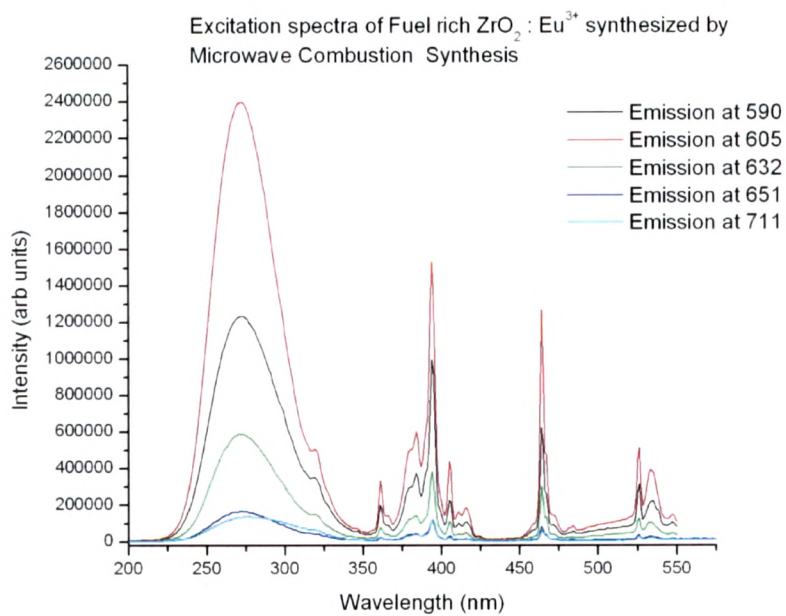


Figure: ZEF5a

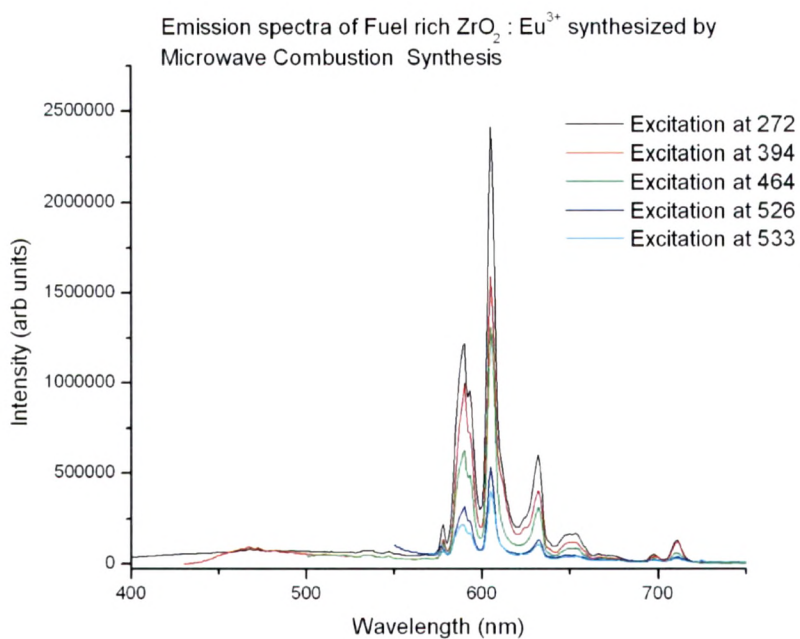


Figure: ZEF5b

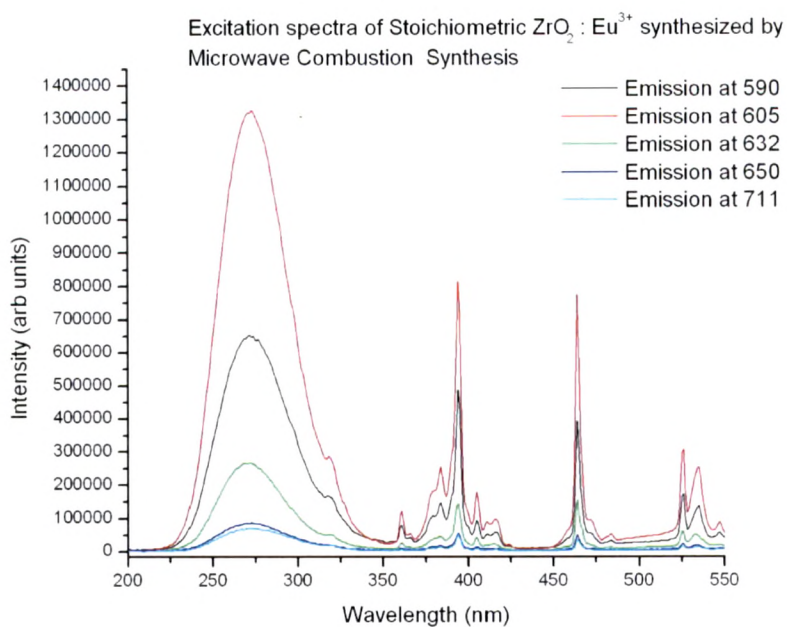


Figure: ZEF6a

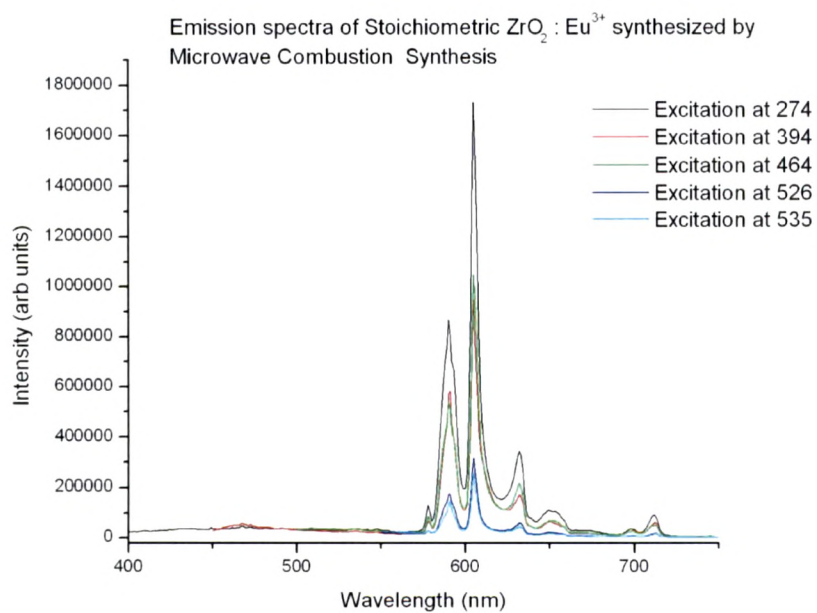


Figure: ZEF6b

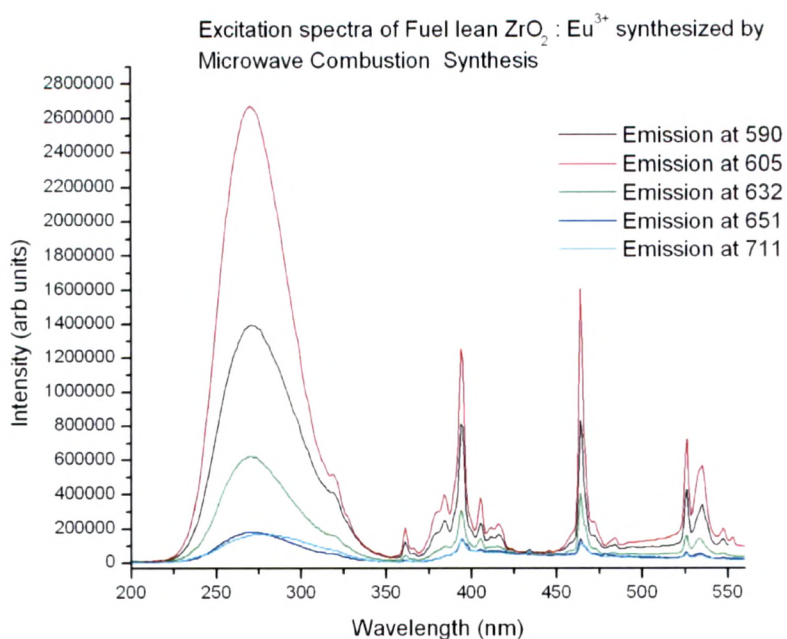


Figure: ZEF7a

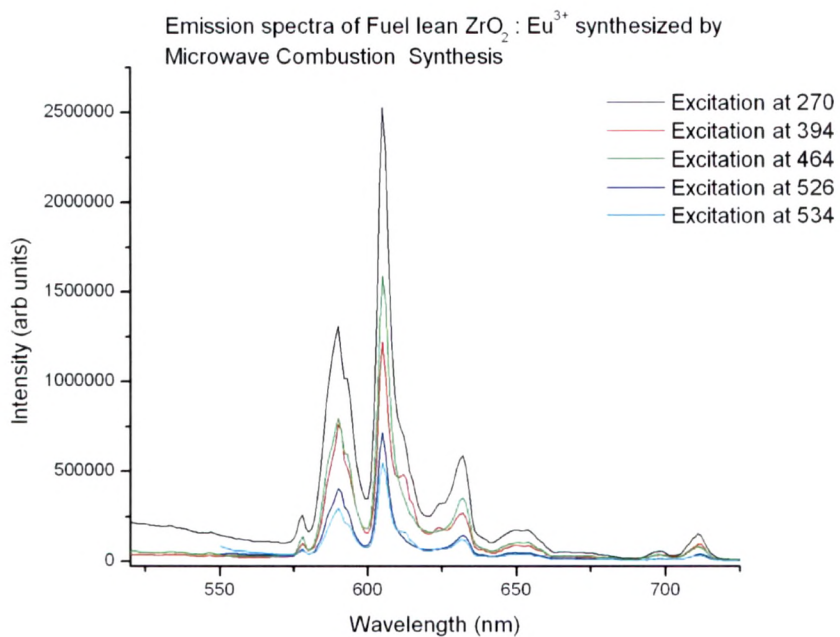


Figure: ZEF7b

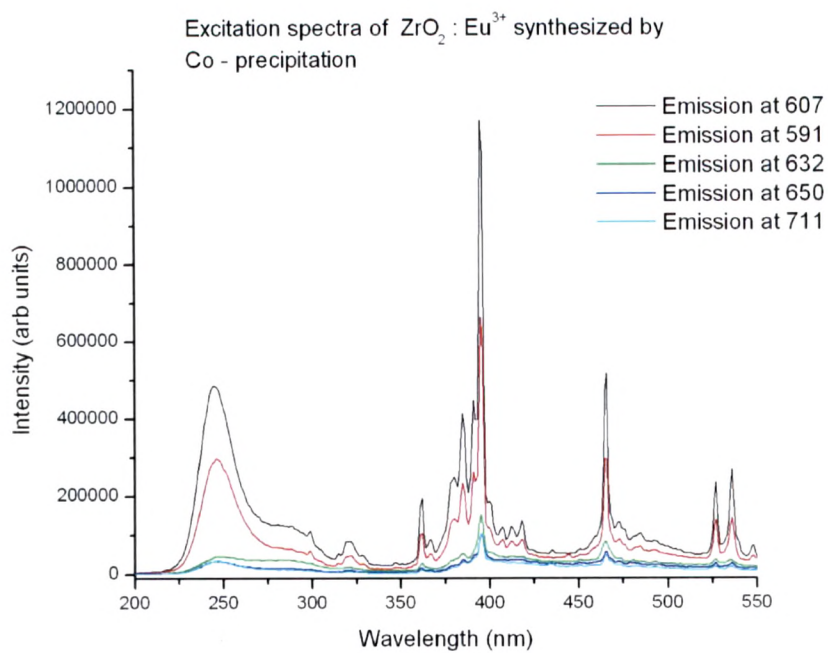


Figure: ZEF8a

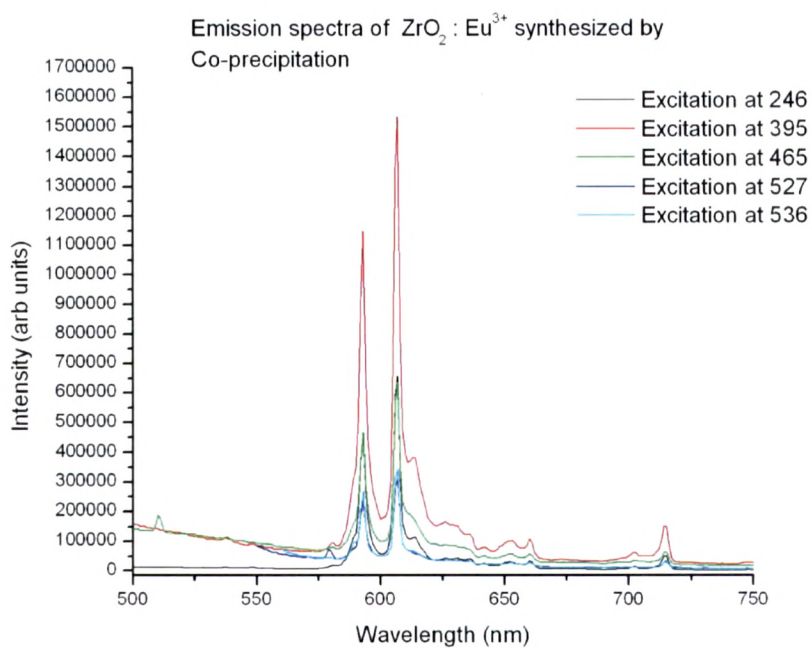
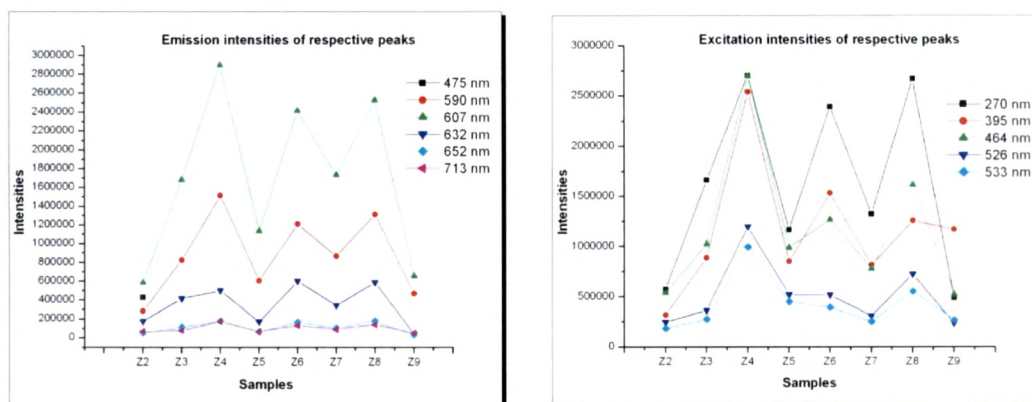


Figure: ZEF8b

The consistency in the spectral patterns is followed by the intensity patterns of the excitation and emission peaks, which are presented graphically as under.



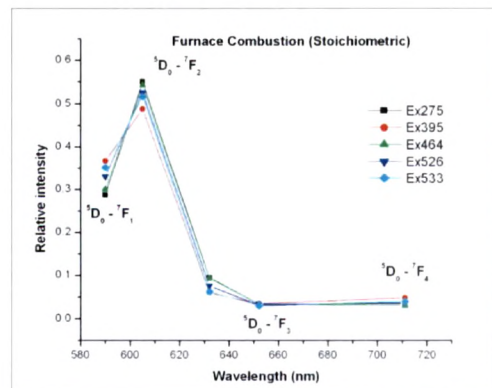
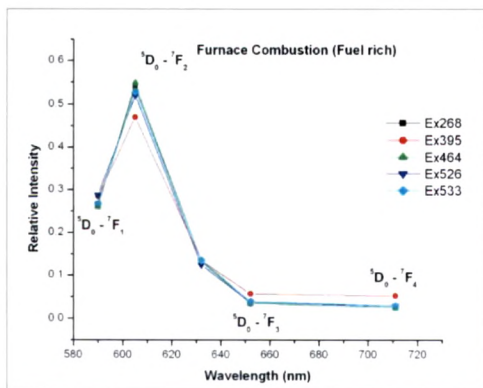
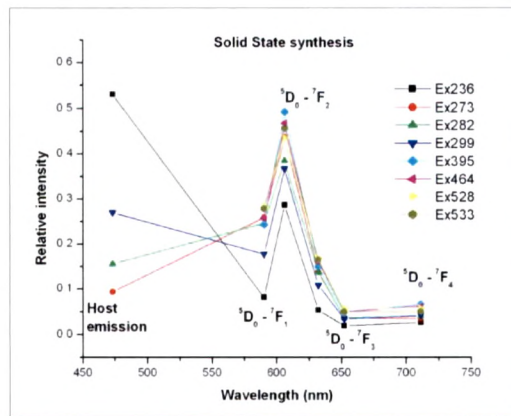
As shown in the figure on left, the highest intensities have been recorded for the emission peak at 607 nm for all the samples. This is followed by the intensity of emission line 590 nm for all the samples, except Z2, where the second highest intensity is for the broad band peak at 475 nm. The intensity variation patterns for both the above mentioned emission peaks is similar. The 590 nm peak emission is due to the ${}^5D_0 \rightarrow {}^7F_1$ magnetic dipole transition while the 607 nm peak is due to the ${}^5D_0 \rightarrow {}^7F_2$ electric dipole transition. The 632 nm peak, also attributed to ${}^5D_0 \rightarrow {}^7F_2$ comes next in terms of intensity. The emission intensities of other peaks for the ${}^5D_0 \rightarrow {}^7F_{3,4}$ transitions have similar variation patterns^[40].

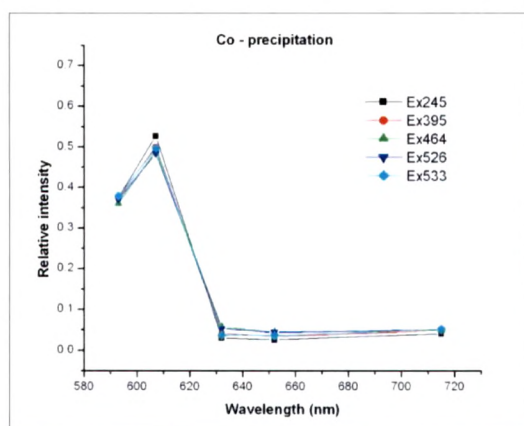
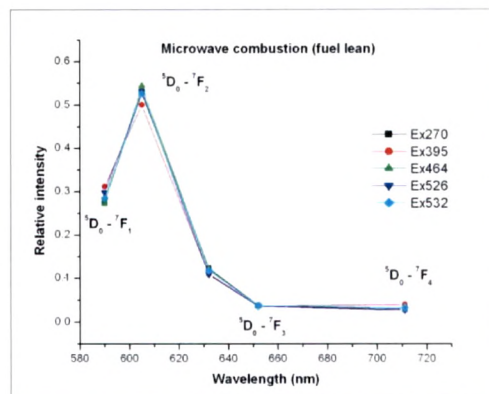
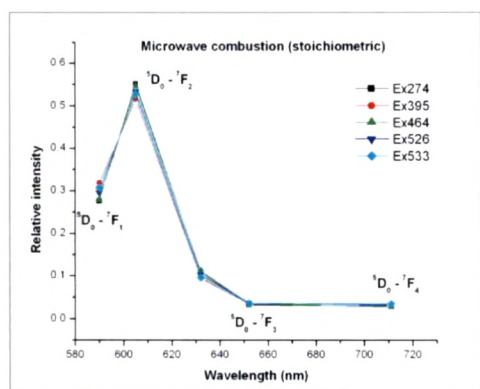
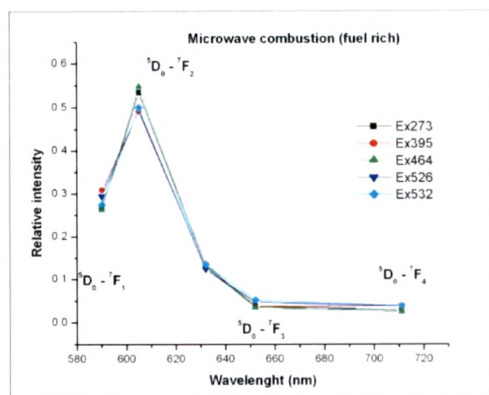
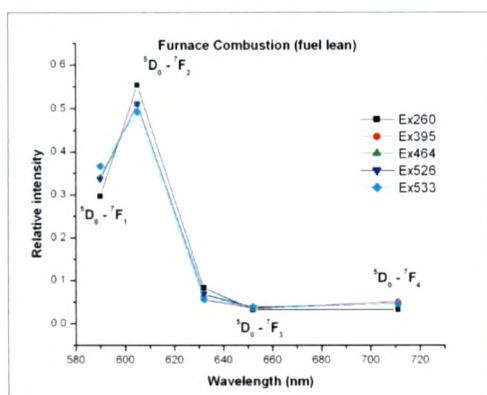
It is observed that the emission intensities are higher for the combustion synthesized samples. The intensities of samples synthesized by solid state and co-precipitation methods are exceptionally low. The highest emission has been recorded for the sample Z4, made by furnace combustion of precursors in stoichiometric proportions. However, combustion of precursors in stoichiometric proportions by microwave assistance does not give high emission yield. In general, the average intensity of furnace made combustion products is higher than the ones made by microwave assistance.

The emission spectra of sample Z2 deserves special attention due to the pronounced broad band emission, which is not seen in any other sample. This is attributed to the host lattice.

The excitation intensities also follow certain trends as is evident from the figure given above on right side. The maximum intensities are for the broad band peaks except for sample Z9, where the most intense peak is at 395 nm. The small particle size seems to enhance the narrow band 395 nm excitation, while curtailing the broad band absorption.

There is good agreement between the excitation and emission intensities indicating high rate of energy transfer from absorption to emission. The distribution of energy among different emission transitions for the respective excitation wavelengths in individual samples is presented below.

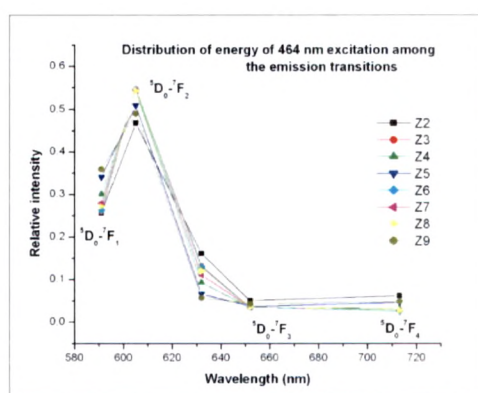
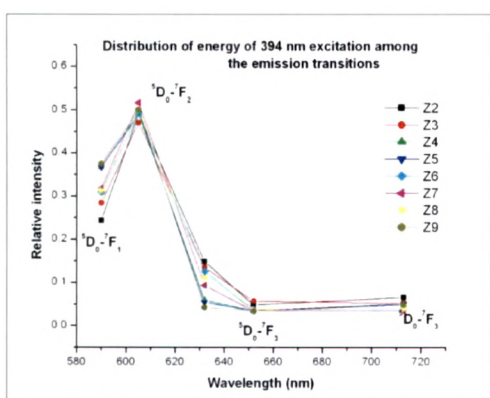
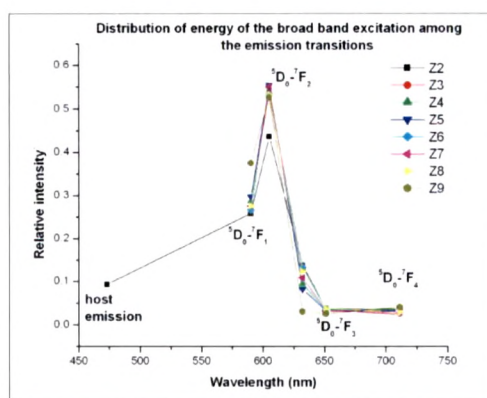


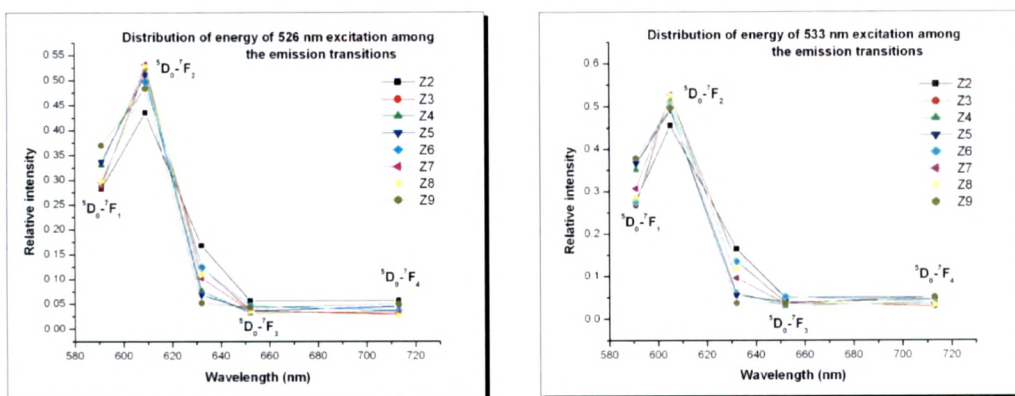


As can be seen from the figures, this distribution is most diverse for the sample prepared by solid state method and the most identical in the case of nano particles. Samples made by combustion synthesis also show a great deal of consistency. The same trend can be seen for the distribution of the individual excitation energies among different emission transitions for all samples collectively, as shown in the figures below.

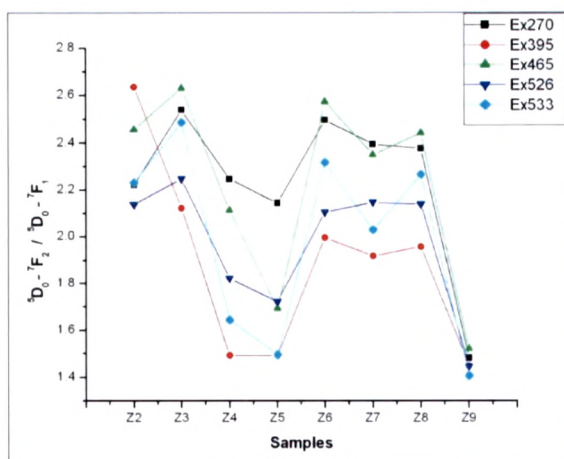
The electric dipole transition ${}^5D_0 \rightarrow {}^7F_2$ acquires the maximum energy in its 607 nm peak for all samples. The magnetic dipole transition ${}^5D_0 \rightarrow {}^7F_1$ at 590 nm also acquires high energy ^[41]. The transfer of energy to the ${}^5D_0 \rightarrow {}^7F_{3,4}$ emission transitions are relatively much low. The proportion of energy transferred to the emission transitions mentioned above is identical for all excitation wavelengths in all samples. The broad band host emission in sample Z2 is also on the lower side.

The energy distribution in case of sample Z9 is restricted to the ${}^5D_0 \rightarrow {}^7F_{1,2}$ transition peaks at 590 nm and 607 nm respectively. Peaks due to transitions ${}^5D_0 \rightarrow {}^7F_{2,3,4}$ at 632, 652 and 713 nm are subjugated. The effect of size reduction seems to be enhancing selective excitation and emission transitions.



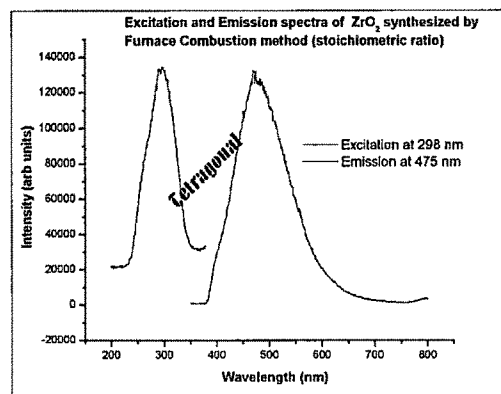
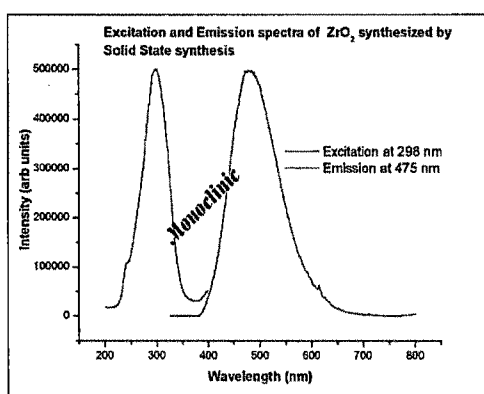


The ratio of intensity of the two peaks i.e. (${}^5D_0 \rightarrow {}^7F_2$ / ${}^5D_0 \rightarrow {}^7F_1$) quantifies the degree of distortion from the inversion symmetry of the local environment of Eu^{3+} ions in the host lattice^[42]. This ratio for the various excitation wavelengths are given below.



The values show substantial variation from sample to sample. The diverse and high values for different excitations of sample Z2 indicate the distribution of Eu^{3+} ions at sites devoid of inversion symmetry being dominant, unlike sample Z9, where the low values of the ratio converge for all excitations to suggest the high inversion symmetry of Eu^{3+} ion distribution. For the combustion synthesized samples, the ratio varies widely for different excitations of the same sample and between samples as well. The 395 nm excitation peak has the highest ratio for sample Z2, suggesting that a large chunk of the excitation energy is taken up by the electric dipole transitions. For the combustion made samples, this peak has the lowest ratio indicating a better order in their crystal lattice. The nano particle sample has the lowest degree of distortion.

The different spectral positions of the broad band excitation features and the subsequent broad band host emission in sample Z2 provides further insight into the excitation and emission mechanism in Zirconia. To investigate the role of the host lattice, two samples of Zirconia were synthesized without any activator, one by solid state method and the other by furnace combustion method in stoichiometric proportions. The former is a proven method to get Zirconia in monoclinic phase while the later gives Zirconia in the tetragonal phase, owing to the high temperatures attained during the process. The excitation and emission spectra of these two samples are given below. Both have identical values of peak excitation as well as emission at 298 nm and 475 nm respectively.



This proves that Zirconia has identical host excitation and emission properties for monoclinic as well as tetragonal phase. However, these properties change when the lattice is activated by Europium. While the monoclinic phase shows host excitation as well as emission, the host emission is completely erased in tetragonal samples.

A close look at the excitation spectra of sample Z2 show charge transition bands apart from host absorption. These broad band features have varying spectral positions from 236 nm to 299 nm. The shift in the spectral position of the charge transfer bands is due to the $\text{Eu}^{3+} - \text{O}$ distance. [Hoefdraad et al.] The shorter the $\text{Eu}^{3+} - \text{O}$ distance, the larger the energy difference between the 4f electrons of Eu^{3+} and 2p electrons of O^{2-} is. Thus, the blue shifts can be attributed to the shorter $\text{Eu}^{3+} - \text{O}$ distance in the respective

samples. The excitation spectra indicates that the emission transitions for peaks at 475, 613 and 624 nm acquire energy from the same excitation line around 298 nm, which is the peak for host excitation. Hence, these emission peaks are due to the host excitation while the other emission lines correspond to excitation broad bands having lower wavelengths, which are formed by the charge transfer states. The excitation spectrum for the 613 nm emission line has another well defined minor broad band feature at 236 nm apart from the host excitation. This split in the peaks, which is also observed for some other emission lines, can be attributed to the absorption by two different $\text{Eu}^{3+} - \text{O}$ bond lengths, seen in the monoclinic structure. [] The broad band host emission at 475 nm can be seen only in the sample Z2 having monoclinic structure. This emission is absent in all other samples, which have tetragonal structure. Thus, it can be inferred that activation of Europium in tetragonal structure leads to transfer of the entire absorbed energy to the Eu^{3+} emission transitions, while in case of monoclinic structure, the absorbed energy is distributed between the host as well as Eu^{3+} emission transitions. Since the emission from Europium activated monoclinic Zirconia, particularly for the host excitation around 298 nm, is spread over the visible range, it will appear white.

ZrO₂: Tb³⁺

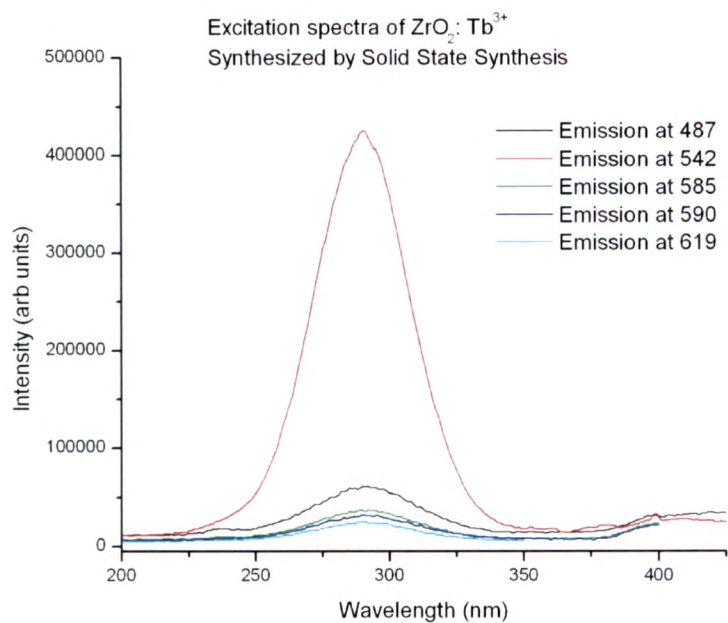
The excitation and emission features of Terbium activated Zirconia are very consistent and on expected lines. Terbium in different hosts is known to give a narrow band green emission. The emission spectra of the samples authenticate this characteristic. The main emission line is centered on 545 nm, the characteristic green emission of Tb^{3+} ions. There are minor features at 487, 585, 590 and 619 nm. The main line shows splitting, with the higher component at 542 nm and the relatively lower one at 249 nm. The emission lines are attributed to $^5\text{D}_4 \rightarrow ^7\text{F}_{3,4,5,6}$ transitions of Tb^{3+} ions.

The excitation spectra of the samples exhibit a single broad band feature. The peak wavelength is at 290 nm. There is a small shift on the lower side, in the peak values for the samples with fuel lean ratio in both kinds of combustion. A major blue shift is observed in case of the sample Z9 consisting of nano particles. This shift, which has

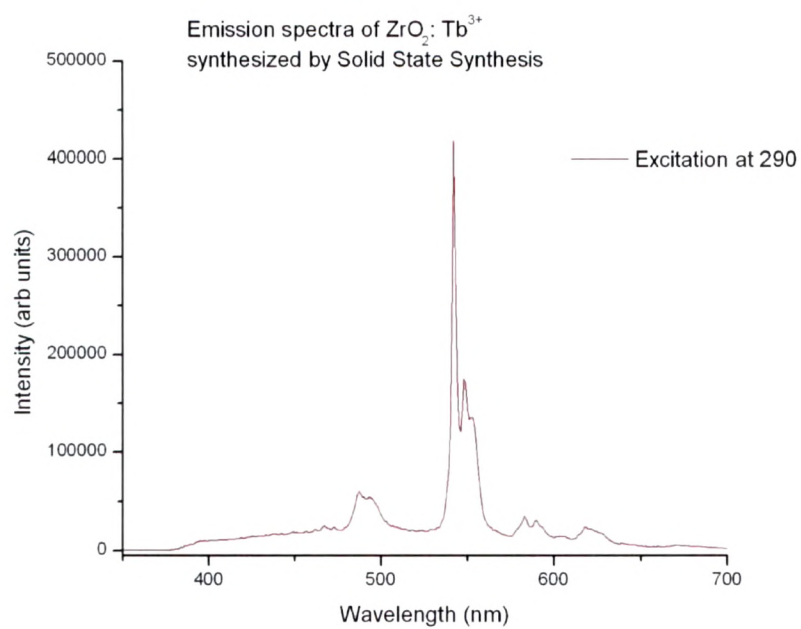
been observed in the photoluminescence spectra of all the samples studied in this work, is attributed to the small particle size and surface effects.

The broad band excitation ranging from 225 nm to 350 nm can be considered to be on account of host absorption, which peaks around 298 nm. It originates from the $4f^8 \rightarrow 4f^75d^1$ transitions. This coincides with the host excitation peak. This band shifts and shrinks in case of the sample Z9 i.e. nano particles. The peak is at 257 nm, giving a sizeable blue shift. A single broad band excitation peak proves that the energy is derived exclusively by the host lattice and is transferred to the Tb^{3+} emission transitions. Unlike Eu^{3+} ions, the Tb^{3+} does not have any narrow band absorption in the Zirconia host lattice.

The characteristic emission of Tb^{3+} is around 545 nm and does not change with host lattice. This consistency is due to the shielding effect, which is prevalent in several rare earth ions and makes them immune to the crystal field effects. The emission at its precise characteristic wavelength and the high intensities of emission indicate the effective incorporation of Tb^{3+} ions in the host matrix. The excitation and emission characteristics of the samples are given below.



ZTF1a



ZTF1b

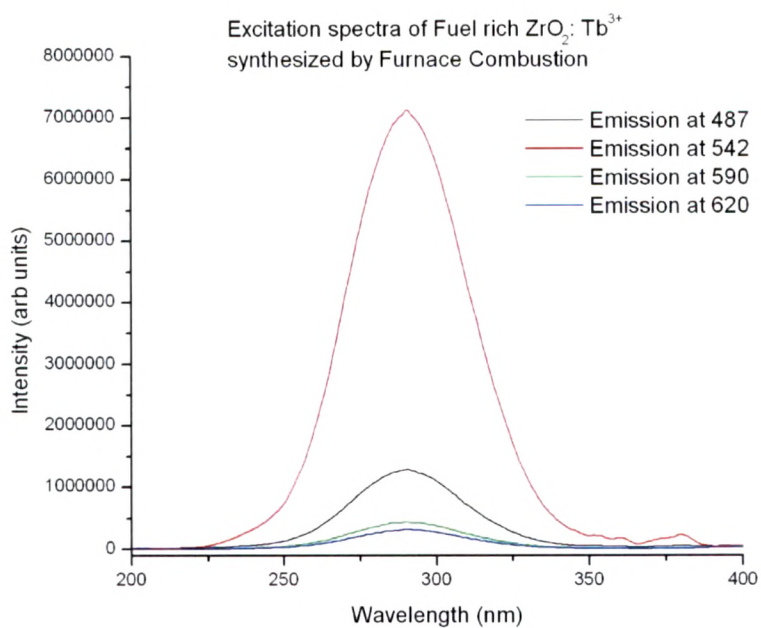


Figure: ZTF2a

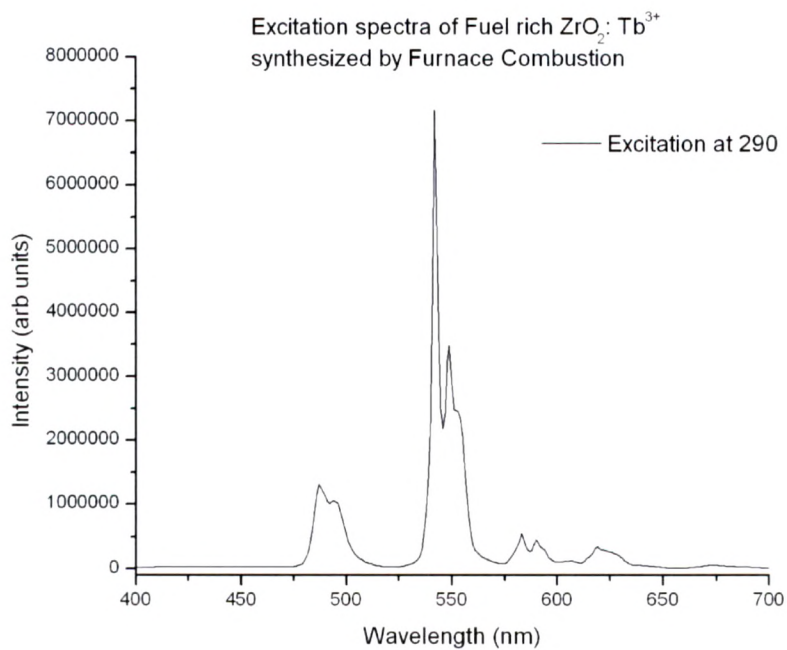


Figure: ZTF2b

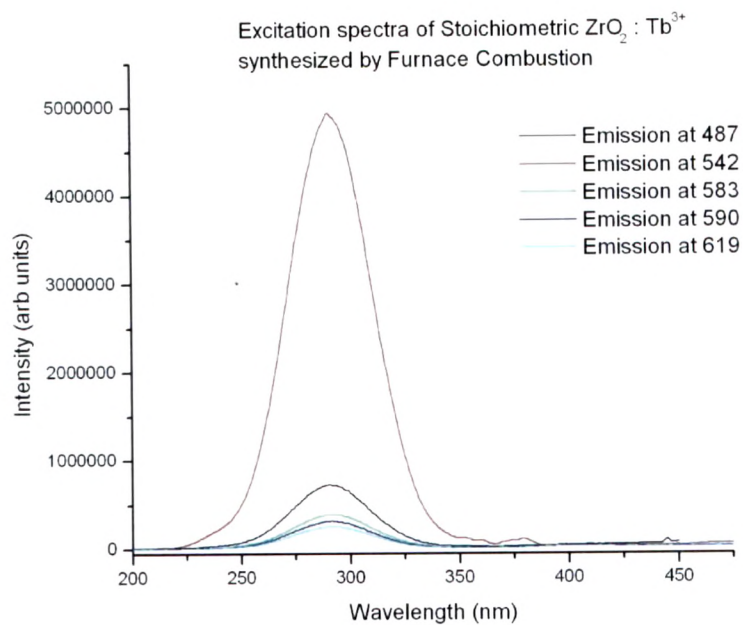


Figure: ZTF3a

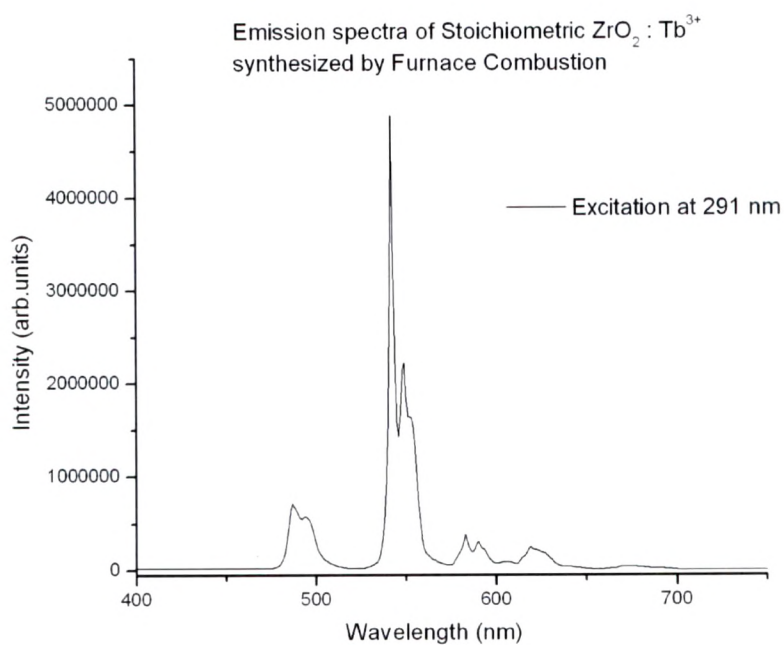


Figure: ZTF3b

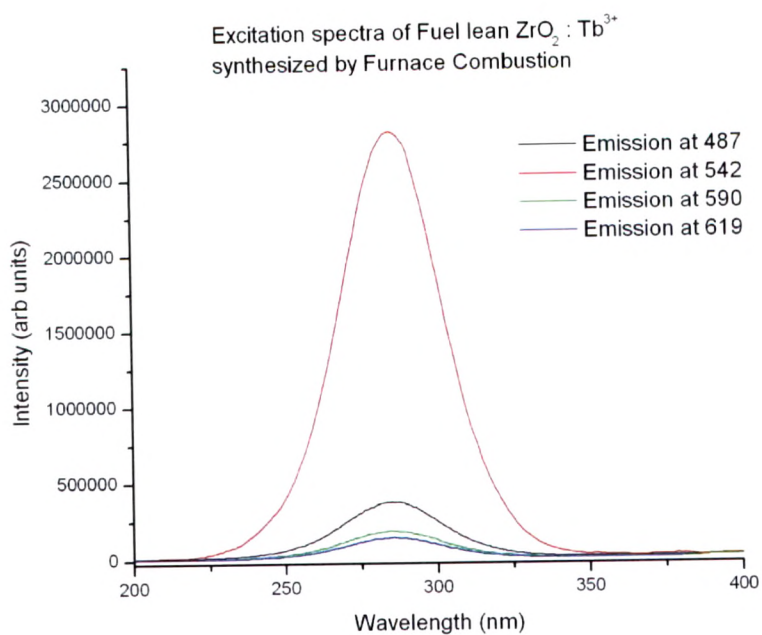


Figure: ZTF4a

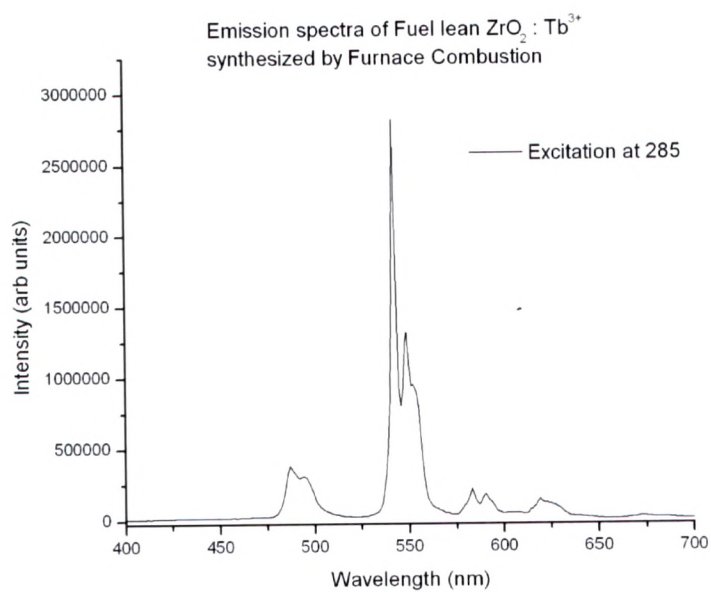


Figure: ZTF4b

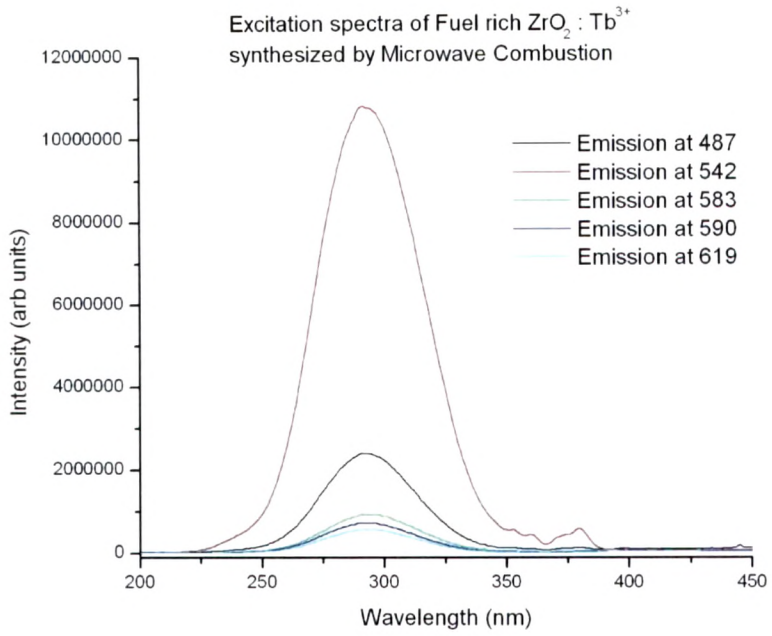


Figure: ZTF5a

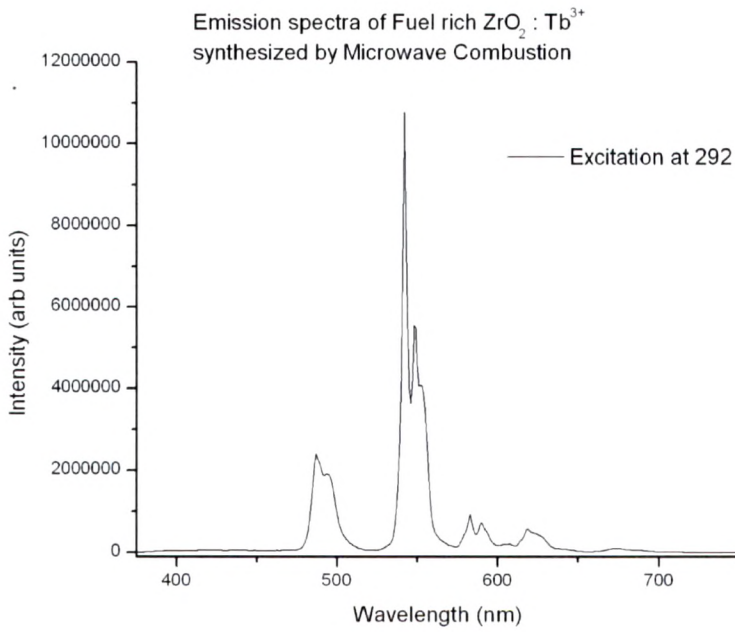


Figure: ZTF5b

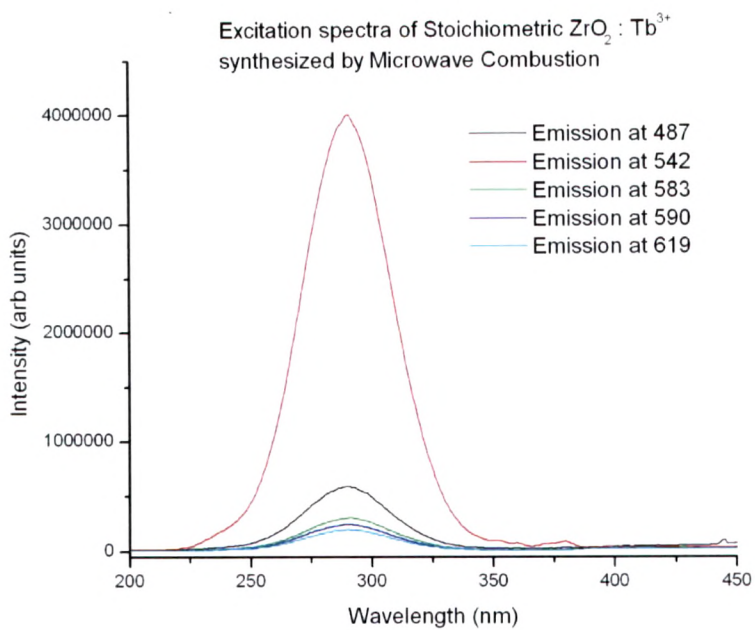


Figure: ZTF6a

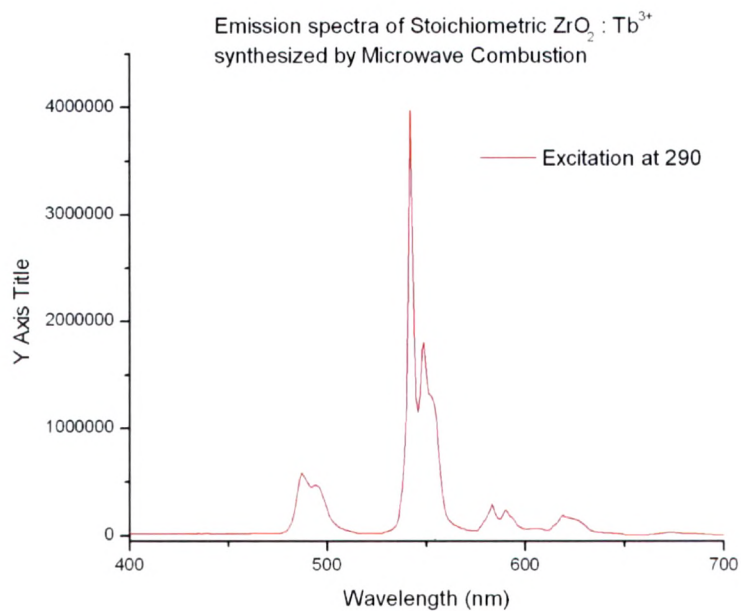


Figure: ZTF6b

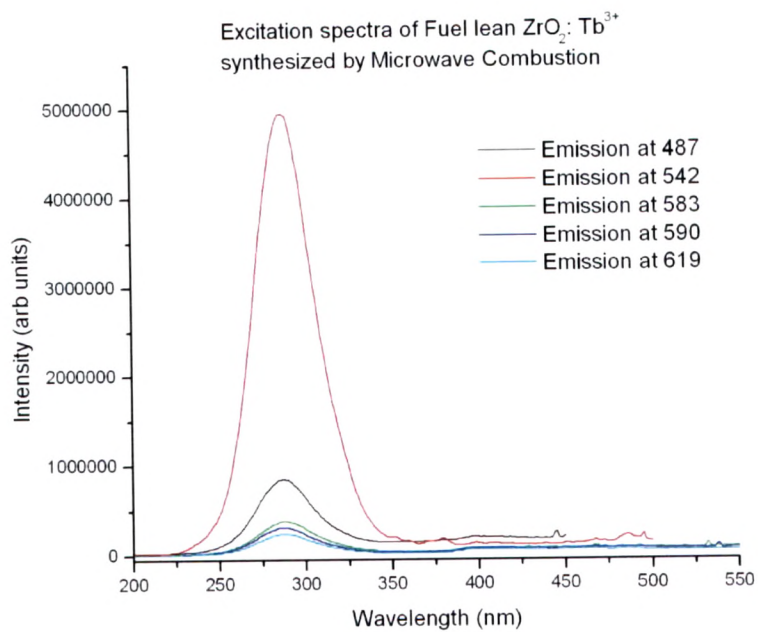


Figure: ZTF7a

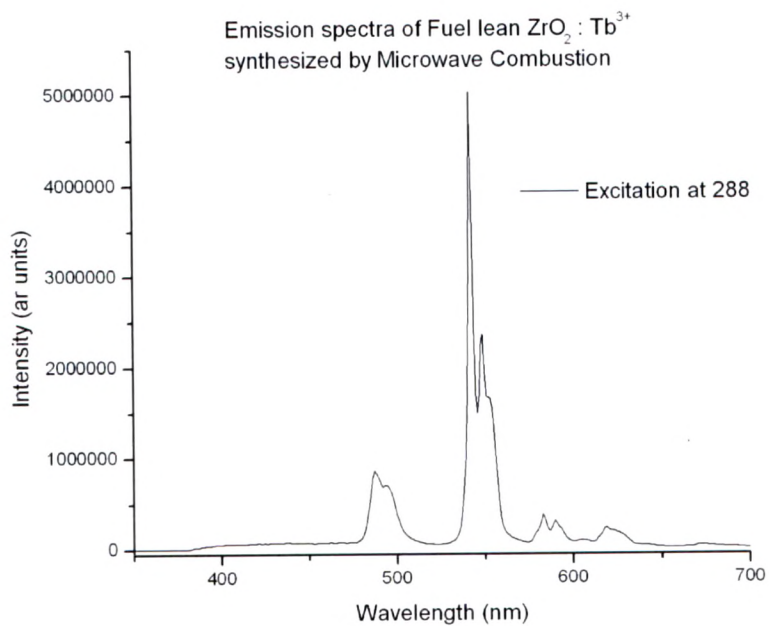


Figure: ZTF7b

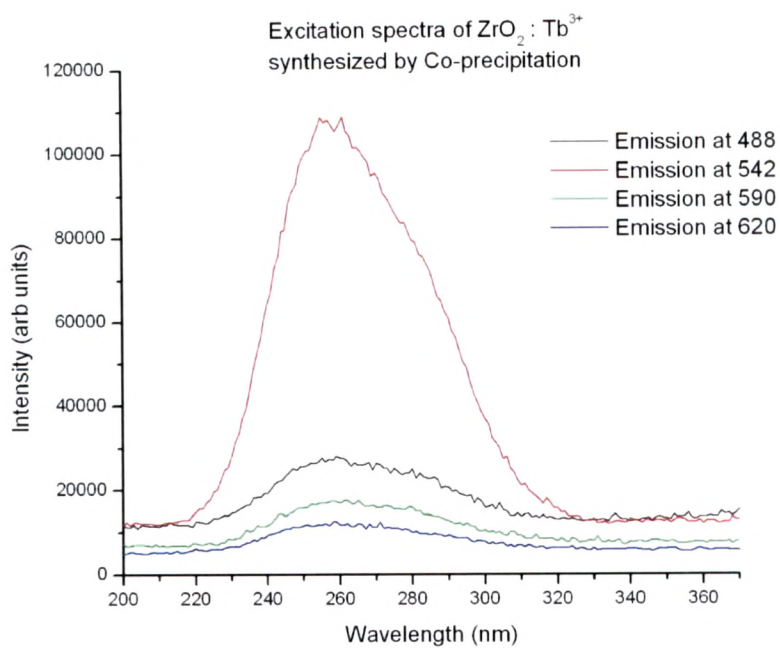


Figure: ZTF8a

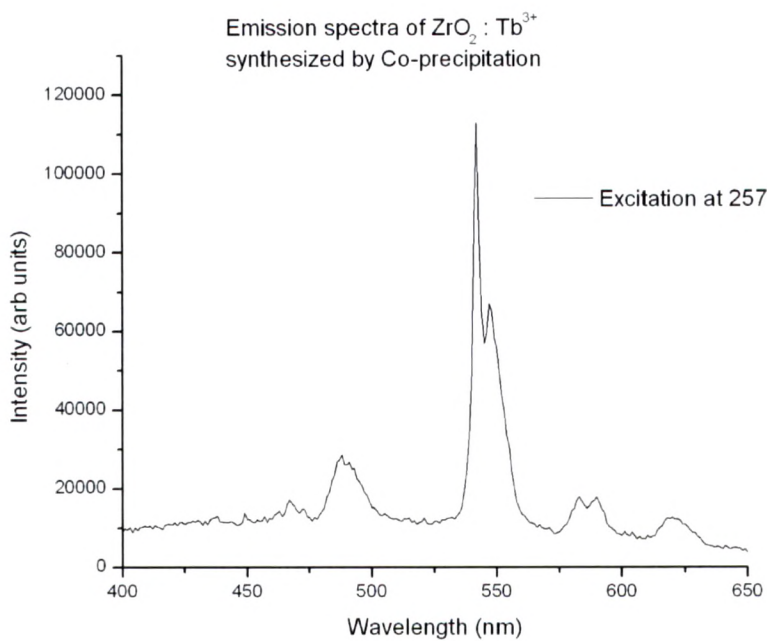
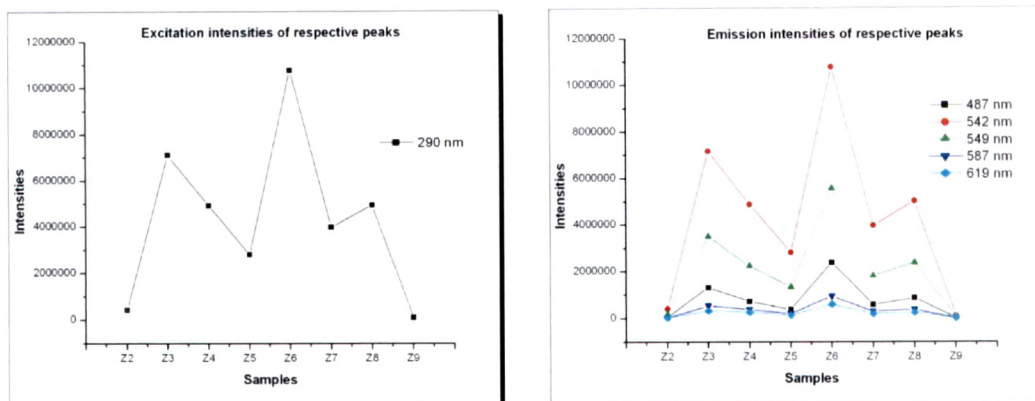


Figure: ZTF8b

The variation of intensities of the excitation and emission peaks is presented below.



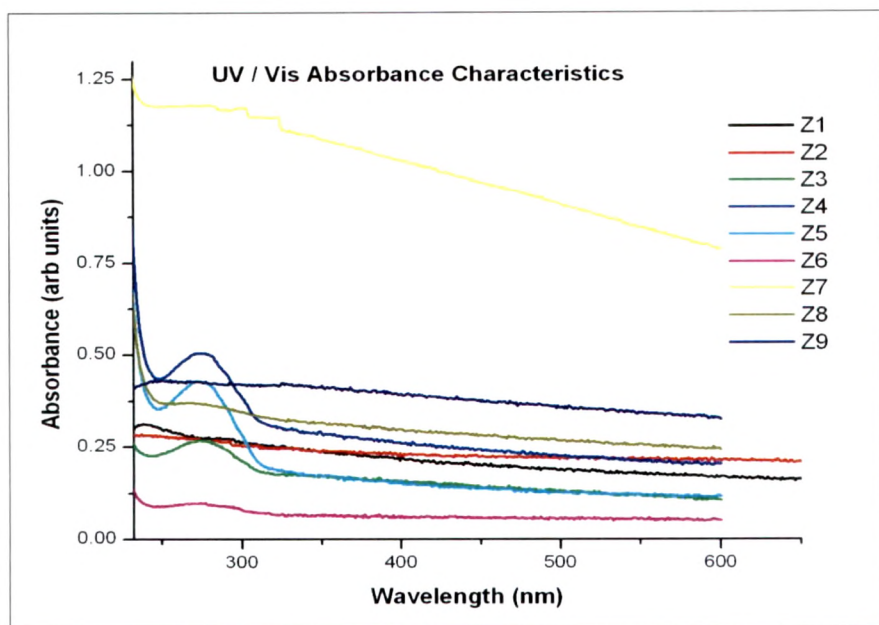
As shown in the figures, the excitation and emission intensities are the lowest for the samples Z2 and Z9, prepared by the solid state and co-precipitation methods respectively. The intensities are comparable in both the samples. The excitation peak for all the samples is at 290 nm except sample Z9. There is a large variation in the intensities of the excitation peaks for the combustion made samples. The highest broad band excitation is seen for the sample Z6 prepared by microwave combustion in fuel rich proportions. In general, the excitation intensities are seen to be higher for samples prepared by microwave combustion as compared to those prepared by furnace combustion.

The intensity of emission lines is almost same for all excitations in case of samples Z2 and Z9, which is a unique feature. The emission intensities show a large degree of variation for different excitation wavelengths in all other samples, which are prepared by combustion synthesis. The highest emission intensity is recorded for sample Z6, prepared by microwave combustion in fuel rich proportions. The emission intensities too are seen to be higher for samples prepared by microwave combustion as compared to those prepared by furnace combustion.

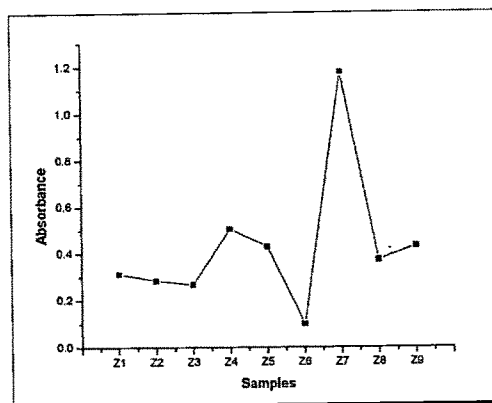
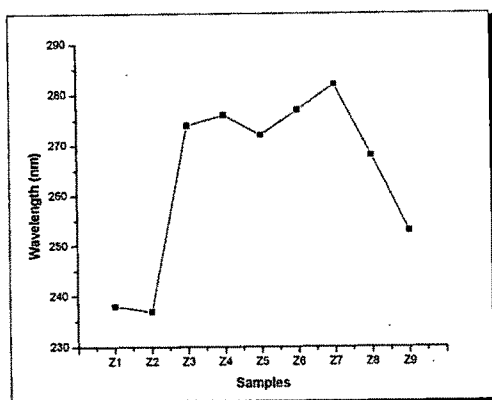
The excitation and emission intensities of the respective samples are comparable as can be seen from the intensity scales of both the figures. This shows that there is efficient conversion of the absorbed energy into the respective emission lines.

UV – Visible Characteristics

The samples taken in equal proportion were dispersed in methanol. Each dispersion was sonicated and then transferred to a quartz cuvette for taking the measurements. The wavelength range was fixed between 230 nm and 600 nm. The results are presented in the figure given below.



Some of the samples show good UV absorption with clear peaks below 300 nm. The variation of absorbance and the peak wavelengths for different samples is given in the figures as under.



Interestingly, the bulk samples Z1 and Z2 have the lowest peak absorption wavelengths and low values of absorbance as well. The combustion made samples have fairly high values of peak absorption wavelengths but their absorbance values show large variations. Both these parameters go hand in hand for the sample Z9. The highest absorbance is seen for sample Z7, prepared by microwave combustion in stoichiometric proportions. The peak absorbance wavelengths are in correspondence with the peak excitation wavelengths.

References

- 1 Garcí'a-Hipo'loto M, Falcony C, Aguilar-Frutis M. A, Azori'n-Nieto, J. *Appl. Phys. Lett.* 2001, 79, 4369
- 2 Fairbanks J W and Hecht R J 1987 *Mater. Sci. Eng.* 88 273
- 3 Di Maggio R, Fedrizzi L, Rossi S and Scardi P 1996 *Thin Solid Films* 286 127
- 4 Harrison H D E, McLamed N T and Subbarao E C 1962 *J. Electrochem. Soc.* 110 23
- 5 Mcleod H A 1986 *Thin Film Optical Filters* 2nd edn (Bristol: Hilger) p 519
- 6 Thomas I M 1994 *Proc. SPIE* 2288 50
- 7 Salas P, De la Rosa-Cruz E, Mendoza D, Gonzales P, Rodr'iguez R and Casta~no V M 2000 *Mater. Lett.* 45 241
- 8 Salas P, De la Rosa-Cruz E, Mendoza-Anaya D, Gonz'alez-Mart'inez P, Casta~no V M and Rodr'iguez R 2000 *Mater. Res. Innov.* 4 452
- 9 Urlacher C, Dumas J, Serughetti J, Mugnier J and Mu~noz M 1997 *J. Sol-Gel Sci. Technol.* 8 999
- 10 Urlacher C, Marco de Luca C, Bernstein E, Jacquier B and Mugnier J 1999 *Opt. Mater.* 12 19
- 11 Zevin M and Reisfeld R 1997 *Opt. Mater.* 8 37
- 12 Savoini B, Mu~noz Santiuste J E and Gonzales R 1997 *Phys. Rev. B* 10 5856
- 13 Altman J C, Stone R E, Dunn B and Nishida F 1991 *IEEE Photonics Technol. Lett.* 3 189
- 14 Y. Sorek, M. Zevin, R. Reisfeld, T. Hurvita, and S. Ruschin, *Chem. Mater.* 9, 670, 1997
- 15 P. Salas, E. De la Rosa-Cruz, D. Mendoza, P. Gonzales, R. Rodr'iguez, and V. M. Casta~no, *Mater. Lett.* 45, 241 ~2000
- 16 Shukla, S.; Seal, S.; Vij, R.; Bandyopadhyay, S. *Nano Lett.* 2003, 3, 397
- 17 Drennan, J. J. *Mater. Synth. Process.* 1998, 6, 181-189
- 18 Haefele, E.; Kaltenmaier, K.; Schoenauer, U. *Sens. Actuators B* 1991, 4, 525-527
- 19 Yamaguchi, T. *Catal. Today* 1994, 20, 199-218
- 20 Turlier, P.; Dalmon, J. A.; Martin, G. A.; Vergnon, P. *Appl. Catal.* 1987, 29, 305-310

- 21 Pavlik, R. S., Jr.; Klein, L. C.; McCauley, R. A. *J. Am. Ceram. Soc.* 1995, 78, 221-224
- 22 Porter, D. L.; Evans, A. G.; Heuer, A. H. *Acta Metallogr.* 1979,27, 1649-1654
- 23 Li, P.; Chen, I.-W.; Penner-Hahn, J. E. *J. Am. Ceram. Soc.* 1994,77, 1281-1288
- 24 Garvie, R. C. *J. Phys. Chem.* 1965, 69, 1238-1243
- 25 Shukla S, Seal S, Vanfleet R, *J. Sol.-Gel Sci. Technol.* 2003, 27, 119
- 26 Mitsuhashi, T.; Ichiara, M.; Tatsuke, V. *J. Am. Ceram. Soc.* 1974, 57, 97-101
- 27 Morgan, P. E. D. *J. Am. Ceram. Soc.* 1984, 67, C-204-C-205
- 28 Wyckoff, R. W.G. (1963) *Crystal Structures: Inorganic Compounds*. New York: Interscience Publishers
- 29 Lauren E Shea, John McKittrick and Olivia A Lopez, *J. of Am. Ceram. Soc.* 79, 1996 3257-65
- 30 S.T. Aruna and K.C. Patil, *NanoStructured Materials Vol. 10. No. 6.* pp. 955-964.1998
- 31 E. C. Subbarao, H. S. Maiti, and K. K. Srivastava, *Phys. Status Solidi A*, 21 (1975)
- 32 R. C. Garvie, *J. Phys. Chem.*, 69, 1238 (1965)
- 33 Garvie, R. C.; Goss, M. F. *J. Mater. Sci.* 1986, 21, 1253-1257
- 34 Garvie, R. C. *J. Am. Ceram. Soc.* 1978, 82, 218-224
- 35 Chraska T, King A. H, Berndt, C. C, *Mater. Sci. Eng. A* 2000, 286, 169-178
- 36 Satyajit Shukla and Sudipta Seal, *J. Phys. Chem. B* 2004, 108, 3395-3399
- 37 N Arul Dhas, K C Patil, *Journal of Solid State Chemistry* 102,1993, pg 440-445
- 38 P. RAVINDRANATHAN, G. V. MAHESH, AND K. C. PATIL, *Journal of Solid State Chemistry* 66,1987, pg 20-25
- 39 M Kitiwan, D Aton, *JSME international Journal Series A Vol. 49 No. 1*, 2006
- 40 Beatriz Juli'an, Rosa Corber'an, Eloisa Cordoncillo, Purificaci'on Escribano, Bruno Viana and Cl'ement Sanchez1, *Nanotechnology* 16 (2005) 2707-2713
- 41 Byung Kee Moona, Il Min Kwona, Jung Hyun Jeonga, Chung-Sik Kimb, Soung-Soo Yic,

- Pyoung Suk Kimd, Haeyoung Choid, Jung Hwan Kimd, *J. of Lum.* 122–123 (2007) 855–857
- 42 Zifeng Qiu, Yuanyuan Zhou, Mengkai Lu, Juan Zhou, Aiyu Zhang, Zhongsen Yang and Qian Ma, *Nanotechnology* 18 (2007) 495705
- 43 Cuikun Lin, Cuimiao Zhang, and Jun Lin, *J. Phys. Chem. C* 2007, 111, 3300-3307
- 44 H. Hoefdraad, M. Steglman and G. Blasse, *Chem. Phys. Lett.*, 1975, 32, 216
- 45 Jianguo Zhoua, Fengying Zhaoa, Xin Wangb, Zhenquan Lia, Yan Zhanga, Lin Yang, *J. of Lum.*, (article in press)